THE JOURNAL OF BIOLOGICAL CHEMISTRY VOL. 290, NO. 47, pp. 28515–28529, November 20, 2015

The Protein Complex of Neurodegeneration-related Phosphoinositide Phosphatase Sac3 and ArPIKfyve Binds the Lewy Body-associated Synphilin-1, Preventing Its Aggregation*

Received for publication, June 5, 2015, and in revised form, September 14, 2015 Published, JBC Papers in Press, September 24, 2015, DOI 10.1074/jbc.M115.669929

Ognian C. Ikonomov[‡], Diego Sbrissa[‡], Lauren M. Compton[‡], Rita Kumar[‡§], Ellen J. Tisdale[¶], Xuequn Chen[‡], and Assia Shisheva[‡1]

From the Departments of [‡]Physiology, [§]Emergency Medicine, and [¶]Pharmacology, Wayne State School of Medicine, Detroit, Michigan 48201

Background: The cytosolic ArPIKfyve-Sac3 complex binds PIKfyve to regulate housekeeping endosomal functions but other tissue-specific interactors and functions are unknown.
Results: Brain Synphilin-1 is a novel interaction partner of the ArPIKfyve-Sac3 complex.
Conclusion: The ArPIKfyve-Sac3 complex is an effective inhibitor of aggregate formation by Synphilin-1.
Significance: The novel molecular means for reducing cytoplasmic aggregates of Synphilin-1 provides new insights into neurodegeneration mechanisms.

The 5-phosphoinositide phosphatase Sac3, in which loss-of-function mutations are linked to neurodegenerative disorders, forms a stable cytosolic complex with the scaffolding protein ArPIKfyve. The ArPIKfyve-Sac3 heterodimer interacts with the phosphoinositide 5-kinase PIKfyve in a ubiquitous ternary complex that couples PtdIns(3,5)P_2 synthesis with turnover at endosomal membranes, thereby regulating the housekeeping endocytic transport in eukaryotes. Neuron-specific associations of the ArPIKfyve-Sac3 heterodimer, which may shed light on the neuropathological mechanisms triggered by Sac3 dysfunction, are unknown. Here we conducted mass spectrometry analysis for brain-derived interactors of ArPIKfyve-Sac3 and unraveled the α-synuclein-interacting protein Synphilin-1 (Sph1) as a new component of the ArPIKfyve-Sac3 complex. Sph1, a predominantly neuronal protein that facilitates aggregation of α-synuclein, is a major component of Lewy body inclusions in neurodegenerative α-synucleinopathies. Modulations in ArPIKfyve/Sac3 protein levels by RNA silencing or overexpression in several mammalian cell lines, including human neuronal SH-SY5Y or primary mouse cortical neurons, revealed that the ArPIKfyve-Sac3 complex specifically altered the aggregation properties of Sph1-GFP. This effect required an active Sac3 phosphatase and proceeded through mechanisms that involved increased Sph1-GFP partitioning into the cytosol and removal of Sph1-GFP aggregates by basal autophagy but not by the proteasomal system. If uncoupled from ArPIKfyve elevation, overexpressed Sac3 readily aggregated, markedly enhancing the aggregation potential of Sph1-GFP. These data identify a novel role of the ArPIKfyve-Sac3 complex in the mechanisms controlling aggregate formation of Sph1 and suggest that Sac3 protein deficiency or overproduction may facilitate aggregation of aggregation-prone proteins, thereby precipitating the onset of multiple neuronal disorders.

The mammalian phosphatidylinositol (3,5)P_2 (PtdIns(3,5)P_2)[2] 5-phosphatase Sac3 (gene symbol *FIG4*) and the scaffolding protein ArPIKfyve (gene symbol *VAC14*) make a stable cytosolic complex that could spatially and temporarily interact with other proteins (1). Thus far, the only known interactor is PIKfyve (gene symbol *PIKFYVE*), the kinase that synthesizes the low abundance signaling lipids PtdIns(3,5)P_2 and PtdIns5P (1–4). In the ternary PAS complex (PIKfyve-ArPIKfyve-Sac3), the ArPIKfyve-Sac3 dimer activates PIKfyve at endosomal membranes, where it couples PtdIns(3,5)P_2, and likely PtdIns5P, synthesis with turnover. PIKfyve, ArPIKfyve, and Sac3 are all evolutionarily conserved proteins encoded by single genes located on human chromosomes 2, 16, and 6, respectively (5). Importantly, the binary ArPIKfyve-Sac3 complex, in addition to binding and activating PIKfyve, has a profound effect on stabilizing the Sac3 protein in the cytosol. This prevents rapid clearance of Sac3 by the ubiquitin-proteasome system, extending the half-life and increasing the steady-state levels of the phosphatase (6). Concordantly, knockdown or knock-out of ArPIKfyve results in reduced or undetectable levels of Sac3 (1, 5–7). Furthermore, work by us and others has found that the primary molecular defect underlying the pathogenesis of hereditary demyelinating neuropathy CMT4J, a disease caused by compound heterozygosity with one null Sac3 allele and one

* This work was supported by National Institutes of Health Grants DK58058 (to A. S.) and GM068813 (to E. J. T.). This work was also supported by Wayne State University, the Wayne State University School of Medicine Research Offices, and the American Diabetes Association 7-13-BS-161 (to A. S.). The authors declare that they have no conflicts of interest with the contents of this article.
[1] To whom correspondence should be addressed: Dept. of Physiology, Wayne State University School of Medicine, 540 E. Canfield Ave., Detroit, MI 48201. Tel.: 313-577-5674; Fax: 313-577-5494; E-mail: ashishev@med.wayne.edu.

[2] The abbreviations used are: PtdIns, phosphatidylinositol; ArPIKfyve, associated regulator of PIKfyve; ArS, ArPIKfyve-Sac3; CMT4J, Charcot-Marie-Tooth type 4J; PAS, PIKfyve-ArPIKfyve-Sac3; PD, Parkinson disease; GFAP, glial fibrillary acidic protein; RIPA, radioimmune precipitation assay; 3-MA, 3-methyladenine.

missense Ile^{41}-to-Thr mutation, is a failure in the ArPIKfyve-dependent protection mechanism toward the Sac3^{I41T} mutant form (6, 8, 9). This leads to rapid Sac3^{I41T} turnover and practically undetectable Sac3 levels in CMT4J patients (6, 10).

Sac3 deficiency has also been implicated as a pathogenic cause and/or a risk factor in other heritable neurological disorders such as amyotrophic lateral sclerosis, with heterozygous null mutations (11–13), Yunis-Varon syndrome, with biallelic null mutations and complete loss of Sac3 (14, 15), and bilateral temporo-occipital polymicrogyria, with homozygous A783V missense mutation (16) within the ArPIKfyve-binding region (2). The ubiquitous presence of the endogenous PAS complex in mammalian tissues and cells (3, 17) together with the ubiquitous ArPIKfyve/Sac3 protein distribution (3, 18, 19) raises the question as to how Sac3 deficiency in both patients and genetically modified null mice results in predominant neuronal defects, whereas other organs remain largely unaffected. Analogously, *arpikfyve* null mice, which die soon after birth, exhibit profound defects in the nervous system but not in other organs, *i.e.* liver, kidney, lung, heart, etc. (7). By contrast, *pikfyve* hypomorphic mice, which also die soon after birth, have prominent defects not only in the brain but also in all organs tested, including heart, lung, kidney etc., whereas a complete *pikfyve* systemic disruption results in preimplantation mouse embryo death (17, 20). Findings for alterations in steady-state levels of PtdIns(3,5)P_2 in opposite directions in mouse models of CMT neuropathies triggered by disruptions of PtdIns(3,5)P_2 phosphatases Sac3 and MTMR2, respectively, also fail to provide a coherent model for the role of PtdIns(3,5)P_2 in the neuropathological mechanism (21, 22).

We surmised that the soluble ArPIKfyve-Sac3 complex may have yet unknown PIKfyve-independent interactions with neuron-specific proteins that could underlie ArPIKfyve-Sac3 functionality in the nervous system. To this end, here we undertook a proteomic screen of mouse brain lysates using the ArPIKfyve-Sac3 complex as bait and unraveled α-synuclein-interacting protein Synphilin-1 (Sph1) (gene symbol *SNCAIP*) as a new interaction partner of the ArPIKfyve-Sac3 complex. Sph1, a predominantly neuronal protein that promotes aggregation of α-synuclein (α-Syn) (gene symbol *SNCA*), is a major component of inclusion bodies, or Lewy bodies, found in post mortem brain samples of neurodegenerative α-synucleinopathies such as Parkinson's and Lewy body dementia (23–27). We further report that the ArPIKfyve-Sac3 complex has a profound ability to reduce the aggregation potential of Sph1 and shift the aggregated protein toward the soluble form. Remarkably, without ArPIKfyve elevation, overexpressed Sac3 itself readily aggregates, potentiating aggregation of Sph1. Our study has identified a novel mechanism of Sph1 aggregation controlled by the ArPIKfyve-Sac3 complex, suggesting that dysregulation of this mechanism may precipitate the onset of Lewy body pathologies and possibly other neurodegenerative disorders.

Experimental Procedures

Antibodies, siRNAs, cDNA Constructs, and Recombinant Proteins—Polyclonal anti-PIKfyve (R7069), anti-Sac3, anti-ArPIKfyve (WS047) affinity-purified on GST-Vac14-(523–782) peptide, anti-GDI2 (R3361) affinity purified on His$_6$-GDI2, and anti-HA (R4289) antibodies were described previously (3, 19, 28–30). Monoclonal anti-MAP2 antibody (clone AP20) and anti-Myc-producing 9E10.2 hybridoma cells were from Millipore and ATCC, respectively. Polyclonal affinity-isolated anti-GFP (Ab290) and anti-Sph1 antibodies (S5946) were from AbCam and Sigma, respectively. SMARTpool siRNA oligonucleotide duplexes (Dharmacon) targeting human or mouse sequences of ArPIKfyve (M-015729 and M-040510), Sac3 (M-019141 and M-052024), human PIKfyve (M-005058), and control cyclophilin B (D-001136) were characterized elsewhere (1, 3, 19, 29, 31). GFP-, HA-, and Myc-tagged cDNA constructs of ArPIKfyve^{WT}, Sac3^{WT}, or GDI2^{WT} and of point/truncated mutants Sac3^{D488A} and ArPIKfyve-(1–511) were described previously (1–3, 19, 30). Simultaneous expression of His$_6$-ArPIKfyve and Sac3 in insect cells by the MultiBac baculovirus system and the purification of the complex on a nickel-agarose resin were described elsewhere (2). Human Sph1-GFP, Sph1-Myc, and GFP-GFAP constructs were kind gifts from Drs. Michael Sherman, Virginia Lee, and James Goldman, respectively.

Cell Cultures, Treatments, and Transfections—Maintenance of COS7 and HEK293 cells was reported previously (2). The generation, maintenance, and doxycycline (1 μg/ml) treatment of the TetOn HEK293 cell line (23L) to express HA-ArPIKfyve^{WT} were detailed elsewhere (6). Human neuroblastoma SH-SY5Y cell line was from ATTC. Primary cultures of cortical neurons were prepared from E18 mice (C57BL/6J) as we have described elsewhere (32). Briefly, cortical brain tissue was collected in complete Hibernate-E medium at 4 °C and digested with papain (Worthington, LS 03126) for 30 min at 37 °C, which was then inactivated with a trypsin inhibitor (Worthington, LS 003085). Cortical neurons were cultured in neurobasal medium (Invitrogen, 21103) supplemented with B-27, GlutaMax-I, and L-glutamate on poly-D-lysine-coated 22-mm^2 coverslips (placed in 6-well dish) at a density of 2–3 × 10^5 and transfected on day 3 with Sac3-siRNAs or cyclophilin siRNAs (0.08 nmol) using the RNAiMax reagents and protocols from Life Technologies Neurobiology. Forty-eight hours later, the neurons were transfected with the Shp1-GFP cDNA by Lipofectamine 3000 (Invitrogen) at a 0.06% final concentration. Neurons were fixed 24–48 h post-transfection for microscopy. SH-SY5Y and HEK293 cell transfection with the indicated siRNAs was performed by Lipofectamine RNAiMax. Protein knockdown was validated 72 h post-siRNA transfection by Western blotting or quantitative RT-PCR as detailed previously (1, 6) (see below). Transient transfection of COS, SH-SY5Y, and HEK293 cells with the cDNAs indicated in the figure legends was performed by Lipofectamine 3000. Double transfection of the TetOn HEK293 cell line was performed simultaneously with or prior to doxycycline induction of ArPIKfyve expression, as specified in the figure legends. Where indicated, cells were treated for 24 h post-transfection with MG132 (proteasome inhibitor, 5 μM) in the presence or absence of nocodazole (microtubule depolymerization reagent, 5 μM) or with the autophagy inhibitors 3-MA (16 h, 10 mM) and chloroquine (16 h, 100 μM). Control dishes received corresponding vehicle treatments.

qRT-PCR—To quantify the knockdown of Sac3 in primary cortical neurons, 72 h post-siRNA administration by

RNAiMax, total RNA was isolated and transcript levels were determined by qRT-PCR using previously characterized mouse primer pairs for amplification and conditions as detailed elsewhere (6).

Fluorescence and Immunofluorescence Microscopy—Transfected cells, grown on coverslips, were fixed in 4% formaldehyde in PBS and permeabilized (0.5% Triton X-100 in PBS). Cells were stained with the primary and secondary antibodies indicated in the figure legends. Coverslips were mounted on slides using a SlowFade antifade kit (Molecular Probes). Cells were viewed under a Nikon Eclipse TE200 inverted microscope at ×400 magnification using the three standard fluorescence channels (*i.e.* green for GFP, red for Alexa Fluor 568, and blue for Alexa Fluor 350 signals) and the Hoffman modulation contrast system. Images were captured with a SPOT RT slider charge-coupled device camera (Diagnostic Instruments, Sterling Heights, MI) and processed using SPOT 3.2 and Adobe Photoshop CS6. Where indicated, coverslips were observed by motorized inverted confocal microscope (model 1X81, Olympus, Melville, NY) with an Uplan Apo objective. Images were captured using a cooled charge-couple device 12-bit camera (Hamamatsu).

Immunoprecipitation, Immunoblotting, and Protein Fractionation—Cell lysates were collected in RIPA$^+$ buffer (50 mM Tris/HCl buffer, pH 8.0, 150 mM NaCl, 1% Nonidet P-40, and 0.5% sodium deoxycholate), supplemented with 1× protease inhibitors (1 mM phenylmethylsulfonyl fluoride, 5 μg/ml leupeptin, 5 μg/ml aprotinin, 1 μg/ml pepstatin, and 1 mM benzamidine). Lysates from mouse brains (male C57Bl6, 4 months old) were prepared by homogenization in RIPA^{2+} buffer, containing 1 x phosphatase inhibitors (1, 19). Immunoprecipitation with the indicated antibodies was performed with precleared lysates (20,000 × *g*, 15 min, 4 °C) and was carried out for 16 h at 4 °C with protein A-Sepharose CL-4B added in the final 1.5 h of incubation. Immune complexes were washed four times with RIPA$^+$ buffer and then processed by Western blotting. Immunoblotting with the antibodies indicated in the figure legends was performed subsequent to protein separation by SDS-PAGE (6% gels) and electrotransfer onto nitrocellulose membranes as described previously (1, 19). A chemiluminescence kit (Pierce) was used to detect the horseradish peroxidase-bound secondary antibodies. Triton X-100-soluble *versus* Triton X-100-insoluble protein fractions of Sph1-GFP or Myc-Sac3 were evaluated in ArPIKfyve-HEK cells with or without ArPIKfyve induction following previously described protocols (30). Briefly, cells on parallel confluent 35-mm dishes were extracted on ice for 2 min with 0.5% Triton X-100 in PBS containing 1× protease inhibitors or directly solubilized for 10 min at 4 °C in RIPA$^+$ buffer containing 0.1% SDS to obtain Triton-soluble and total protein fractions, respectively. The Triton-insoluble protein fraction that remained on the first dish was then solubilized in RIPA$^+$ buffer containing 0.1% SDS. Equal volumes of the respective fractions were analyzed by immunoblotting with the indicated antibodies.

Sample Preparation and NanoLC-MS/MS Analysis—The Myc-Sac3-HA-ArPIKfyve complex, immunopurified from transfected COS7 cells with a monoclonal anti-Myc antibody and immobilized on protein A-Sepharose CL-4B beads, was incubated with mouse brain lysates for 16 h at 4 °C. Anti-Myc immune complexes immobilized on protein A-Sepharose CL-4B beads derived from lysates of nontransfected or Myc-Sac3-transfected COS7 cells were incubated with brain lysates in parallel and served as controls. After extensive washing in RIPA$^+$ buffer, the beads were analyzed by SDS-PAGE. Gels were stained with SYPRO Ruby reagent (Lonza). Corresponding gel pieces (~2-mm height) from the control and sample lanes with or without visible protein bands were excised starting from the 100-kDa marker (to avoid the strong bands for IgG, ArPIKfyve, or Sac3) up to nearly the top of the gel. In-gel protein digestion and nanoLC-MS/MS analyses were performed as described previously (33, 34). Briefly, gel pieces were washed with 50 mM ammonium bicarbonate, reduced in 10 mM DTT at 37 °C for 45 min, and alkylated with 55 mM iodoacetamide for 30 min at room temperature. Trypsin (sequencing grade) was then added at 10 ng/μl, and digestion was carried out at 37 °C for 14 h. The resulting peptides were separated on a reverse-phase C18 column by HPLC using the Dionex Ultimate^{TM} HPLC system. MS and MS/MS spectra were then acquired on an Applied Biosystems mass analyzer (QSTAR XL) using the information-dependent acquisition mode. An MS scan was performed from m/z (mass-to-charge) 400-1500 for 1 s followed by product ion scans on the two most intense multiply charged ions. Peak lists were submitted to the Mascot server to search against the non-redundant NCBI database for all entries with carbamidomethyl used as a fixed modification and oxidation as a variable modification. A protein was considered a hit if it was identified with at least two peptides.

Other Assays, Quantitation, and Statistics—Quantitation of cells with inclusions was performed by counting 25–100 cells/neurons from >3 randomly chosen fields per condition in three separate experiments and normalized for the number of transfected cells, as specified in the figure legends. Cells or neurons were considered to have multiple aggregates if two or more Sph1-GFP- or Myc-Sac3-positive small cytoplasmic inclusions were detected. Aggresome-positive cells were scored when a single perinuclear inclusion of Sph1-GFP or Myc-Sac3 was observed after proteasome inhibition in a microtubule-sensitive manner. Protein concentration was determined by bicinchoninic acid protein assay (Pierce). Protein levels were quantified from the intensity of the immunoblot bands by a laser scanner (Microtek) and UN-SCAN-IT software (Silk Scientific). Data are presented as mean ± S.E. Statistical analysis was performed using Student's t test, with $p < 0.05$ considered as significant.

Results

Sph1 Interacts with the ArPIKfyve-Sac3 Complex—To identify novel interaction partners of the ArPIKfyve-Sac3 complex in the nervous system, mouse brain lysates were incubated with the ArPIKfyve-Sac3 complex, which was immunopurified using a monoclonal anti-Myc antibody from lysates of COS7 cells transfected with HA-ArPIKfyve-Myc-Sac3. Anti-Myc immunoprecipitates of nontransfected or Myc-Sac3-transfected COS7 cells, processed in parallel, served as controls. Mass spectrometric analysis was performed on gel pieces positioned above the 100-kDa protein band to avoid peptide frag-

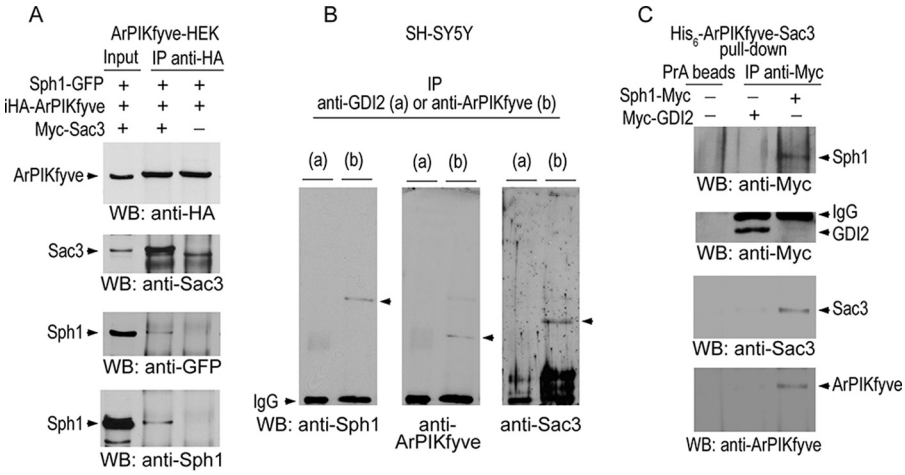

FIGURE 1. **ArPIKfyve-Sac3 complex interacts with Sph1.** *A*, ArPIKfyve-HEK cells were transfected with Sph1-GFP alone or together with Myc-Sac3 when expression of HA-ArPIKfyve was induced (*i*). Twenty-four h post-transfection/induction, the cells were scraped in RIPA$^+$ buffer. Cleared lysates were immunoprecipitated (*IP*) with purified anti-HA IgG and processed by SDS-PAGE and Western blotting (*WB*) as specified under "Experimental Procedures." Shown are chemiluminescence detections of representative blots of three with similar results depicting the three proteins in input lysates and immunoprecipitations. Note the similar amounts of IP ArPIKfyve and that the band of Sph1-GFP (detected by anti-GFP and anti-Sph1 antibodies) is coimmunoprecipitated only when Sac3 is coexpressed/coimmunoprecipitated. *B*, RIPA$^+$ lysate collected from SH-SY5Y neuroblastoma cells were immunoprecipitated with anti-ArPIKfyve or control anti-GDI2 antibodies, affinity-purified on an ArPIKfyve C-terminal peptide and His_6-GDI2 protein, respectively. Immunoprecipitates were processed for SDS-PAGE and Western blotting with a stripping step between the indicated antibodies. Shown are chemiluminescence detections of representative blots of two with similar results, demonstrating specific bands corresponding to Sac3 and Sph1 electrophoretic mobilities (*arrowheads*), coimmunoprecipitated with anti-ArPIKfyve only but not with GDI2 antibodies. *C*, *in vitro* associations of purified recombinant His_6-ArPIKfyve-Sac3 with immunopurified Sph1-Myc. Sph1-Myc and a control, Myc-GDI2, immunopurified on the anti-Myc antibody from RIPA$^+$ lysates of transfected COS7 cells and immobilized on protein A-Sepharose CL-4B (*PrA*) beads were incubated with the His_6-ArPIKfyve/Sac3 complex, purified from infected Sf21 cells on nickel-nitrilotriacetic acid-agarose. PrA beads alone were incubated in parallel. After washing, beads were subjected to SDS-PAGE and Western blotting. Nitrocellulose membranes were probed with anti-Myc and, after a horizontal cut through the middle, with anti-ArPIKfyve and anti-Sac3 antibodies (*lower panels*) with a stripping step in between. Shown are chemiluminescence detections of representative blots of three separate experiments, illustrating efficient pulldown of the purified ArPIKfyve-Sac3 recombinant complex by Sph1-Myc but not by Myc-GDI2 or protein A-Sepharose CL-4B.

ments of ArPIKfyve, Sac3, and/or IgG sequences, which migrated below 100 kDa (not shown). Bioinformatics revealed several potential interactors in the brain, specifically captured by the HA-ArPIKfyve-Myc-Sac3 complex. Among the hits, Sph1 was one of the strongest candidates for two reasons: first, it was reproducibly identified by two specific peptides only in the lane of the ArPIKfyve-Sac3 complex but not in the control lanes; and second, it was retrieved from a gel band in the vicinity of 115–130 kDa, a gel area corresponding to the size of the full-length mouse clone (NP_080684). Human and mouse Sph1 exhibit similar open reading frames of 915 and 919 amino acid residues, respectively, and are highly homologous along the entire protein sequences, with ~97% identity in the ankyrin-like repeats and coiled-coil domain (24, 35).

To confirm the predicted specific interaction, we took advantage of our stable HEK293 cell line expressing human HA-ArPIKfyve upon induction with doxycycline (further as iArPIKfyve-HEK) (6), which provided relatively high efficiency for concurrent expression of the three proteins. Following transfection with human Sph1-GFP cDNA alone or with Myc-Sac3 cDNA and induction of human HA-ArPIKfyve, cell lysates were immunoprecipitated with anti-HA antibodies followed by SDS-PAGE and Western blotting. The membranes were then probed for each of the three proteins. As identified previously (1, 6) and confirmed herein, we recovered Sac3 in ArPIKfyve immunoprecipitates, as the two proteins form a stable complex (Fig. 1*A*). More importantly, however, we recovered Sph1-GFP by either anti-GFP or anti-Sph1 antibodies in the HA-ArPIKfyve immune complex but only if Myc-Sac3 was coexpressed (Fig. 1*A*).

An important aspect is whether the triple interaction occurs in the context of neuronal cells. To address this question, we conducted coimmunoprecipitation analyses with lysates from the human SH-SY5Y neuroblastoma cell line, in which the presence of endogenous Sph1 had been reported previously (36, 37). As illustrated in Fig. 1*B*, we found a coimmunoprecipitated band of Sac3 only in immunoprecipitates of affinity-purified anti-ArPIKfyve antibodies but not in those of affinity-purified GDI2 antibodies, consistent with the established interaction of the endogenous ArPIKfyve-Sac3 proteins (3). More importantly, however, besides Sac3, in ArPIKfyve but not in the GDI2 immunoprecipitates we also retrieved Sph1, evidenced by visualizing a single anti-Sph1 immunoreactive band with electrophoretic mobility of Sph1 (Fig. 1*B*).

We also verified the triple interaction *in vitro* by using a purified His_6-ArPIKfyve-Sac3 complex, produced by a multigene baculovirus system (2) and Sph1-Myc, immunopurified on an anti-Myc antibody from lysates of transfected COS7 cells (Fig. 1*C*). As a control for specificity, we monitored the interaction of the His_6-ArPIKfyve-Sac3 complex with anti-Myc-GDI2 immunoprecipitates derived from COS7 cells transfected in parallel with Myc-GDI2 cDNA. As illustrated in Fig. 1*C*, the purified recombinant His_6-ArPIKfyve-Sac3 complex was recovered only with Sph1-Myc but not with Myc-GDI2. The fact that purified Sph1-Myc pulls down the recombinant ArPIKfyve-Sac3 complex produced in insect cells suggests that the specific interaction between Sph1 and the ArPIKfyve-Sac3 complex occurs directly.

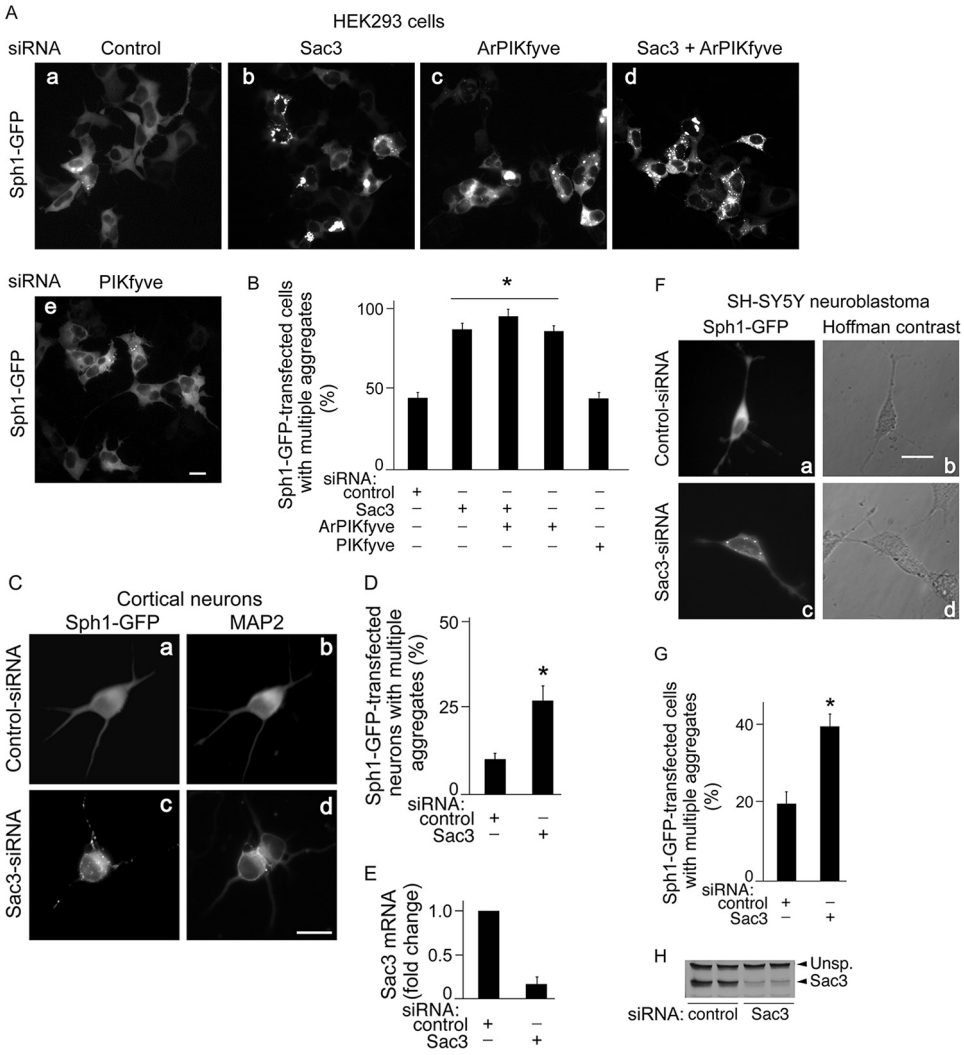

FIGURE 2. **Deficiency of ArPIKfyve and/or Sac3, but not PIKfyve, facilitates aggregation of Sph1-GFP in non-neuronal and neuronal cells.** *A* and *B*, HEK293 cells were transfected with the indicated siRNA duplexes. Forty-eight h post-siRNAs, cells were transfected with cDNA of Sph1-GFP and 24 h later were fixed and processed for fluorescence microscopy as described under "Experimental Procedures." Presented are typical fluorescence microscopy images of Sph1-GFP-positive cells treated with the indicated siRNAs (*A*); the data quantitation is expressed as a percentage of transfected cells with Sph1-GFP aggregates (*B*). The percentage of cells with multiple cytoplasmic aggregates was determined by viewing >100 GFP-positive cells from at least three random fields/condition in three separate experiments. *C–E*, mouse cortical neurons, prepared from E18 mice and cultured on poly-D-lysine-coated glass coverslips for 3 days, were transfected with the indicated siRNA duplexes by RNAiMax as described under "Experimental Procedures." Forty-eight h later, neuronal cultures were transfected with cDNA of Sph1-GFP. Twenty-four to 48 h post-cDNA transfection, the neurons were fixed and processed for immunofluorescence with anti-MAP2 monoclonal, as a primary antibody, and anti-mouse Alexa Fluor 568 as a secondary antibody. Shown are representative fluorescence/immunofluorescence microscopy images of Sph1-GFP-expressing cells, for which the dendrites and soma are visualized by anti-MAP2 (*C*); and the quantitation of the Sph1-GFP aggregation under different conditions as a percentage of the transfected neurons shows depicting multiple small aggregates in soma and dendrites, determined by viewing >25 GFP-positive cells/condition in three separate experiments (*D*). Note that Sph1-GFP is predominantly diffuse in control neurons but forms multiple small aggregates under Sac3 depletion. Total RNA was harvested and analyzed by quantitative RT-PCR for Sac3 mRNA expression as described under "Experimental Procedures" ($n = 3$, $p < 0.001$) (*E*). *F–H*, SH-SY5Y neuroblastoma were transfected with the indicated siRNA duplexes. Forty-eight h later, cells were transfected with cDNA of Sph1-GFP. Twenty-four h post-cDNA transfection, cells were either fixed for fluorescence microscopy (*F*) or lysed for Western blotting analysis (*H*) as described under "Experimental Procedures." Shown are representative fluorescence microscopy images of Sph1-GFP-positive cells treated with the indicated siRNAs, and the corresponding phase image, captured by Hoffman modulation contrast (*F*). Quantitation of the Sph1-GFP aggregation demonstrates a significant increase under Sac3 depletion (*G*). Chemiluminescence detection of a representative blot (in duplicates) of two separate experiments with similar results indicates marked decreases in endogenous Sac3 levels by Sac3-siRNA; the equal intensities of the unspecific bands (*Unsp.*) above Sac3 attest to equal loading (*H*). The percentage of cells with multiple small cytoplasmic aggregates was determined by viewing >50 GFP-positive cells from at least three random fields/condition in three separate experiments. *, significant increase in the proportion of cells with multiple small Sph1-GFP aggregates *versus* control ($p < 0.05$). *Bar*, 10 μm.

ArPIKfyve-Sac3 Deficiency Enhances Aggregation of Sph1—Sph1-GFP is an aggregation-prone protein that, at high levels of ectopic expression, forms multiple cytoplasmic aggregates in several cell types, including HEK293 cells (38, 39). Consistently, along with diffuse distribution, we also observed multiple small aggregates of Sph1-GFP in 40–45% of the transfected HEK293 cells (Fig. 2*A* and *B*). Notably, as complete deficiency of Sac3 leads to the appearance of cytoplasmic inclusions in different cells from both Sac3 KO mice and Yunis-Varon syndrome patients (14, 40), a plausible role of Sac3 loss in protein aggregation could be anticipated. To address the outcome of Sac3 deficiency and, hence, the ArPIKfyve-Sac3 complex deficiency in aggregate formation by Sph1, we monitored the consequences of siRNA-mediated Sac3 protein depletion, alone or

combined with that of ArPIKfyve, in HEK293 cells transiently expressing Sph1-GFP. Consistent with our previous Western blot analyses in these cells (1, 3, 6, 19) confirmed herein (not shown), we observed a 70–90% reduction in Sac3 or ArPIKfyve protein levels 72 h post-transfections with the corresponding human siRNA sequences as well as concomitant decreases in Sac3 protein levels upon ArPIKfyve depletion. Intriguingly, protein depletion of Sac3 or ArPIKfyve had a prominent effect on the aggregation propensity of Sph1, nearly doubling the proportion of cells with multiple small Sph1-GFP aggregates (Fig. 2, *A* and *B*). The two siRNA pools harbor different seed region sequences, underscoring the specificity of the effect. Consistent with the marked reduction of the complex upon ablation of either ArPIKfyve or Sac3, the combined depletion of the two proteins only slightly increased the Sph1-GFP propensity to form multiple aggregates (Fig. 2*B*). By contrast, PIKfyve protein ablation did not significantly alter the proportion of cells with multiple small aggregates of Sph1-GFP (Fig. 2, *A* and *B*), further supporting the notion that the ArPIKfyve-Sac3 complex affects Sph1 aggregative properties independently of the kinase.

To establish whether this increased aggregation of Sph1 at reduced levels of the ArPIKfyve-Sac3 complex is phenocopied in neurons, we knocked down Sac3 in primary E18 mouse cortical neuron cultures using previously validated mouse Sac3-targeting siRNAs (3, 29). The appearance of the expressed Sph1-GFP was compared with that in control neurons receiving siRNAs of mouse cyclophilin. Data quantitation with cortical neurons derived from three pregnancies revealed that in the control condition, expressed Sph1-GFP exhibited primarily a diffuse distribution pattern (Fig. 2, *C* and *D*) in agreement with previous observations in HA-Sph1-transfected cortical neurons (41). However, we detected aggregates of Sph1-GFP in ~10% of the transfected neurons (Fig. 2, *C* and *D*). Intriguingly, under Sac3 depletion, evidenced by markedly reduced Sac3 mRNA levels (Fig. 2*E*), the number of Sph1-GFP-positive neurons with multiple small aggregates was markedly increased (Fig. 2*D*). The aggregates were seen scattered throughout both the soma and dendrites, as revealed by staining with the neuronal marker MAP2 (Fig. 2*C*).

To further validate the above observation for human neurons, we sought to explore the widely used human SH-SY5Y neuroblastoma cell line, where expressed Sph1-GFP was reported to have a diffuse distribution in the majority of transfected cells (42). Consistently, under control transfection with cyclophilin siRNA, we also observed a diffuse pattern of Sph1-GFP expression in most of the transfected cells, with ~20% of the cells exhibiting multiple small Sph1-GFP-positive aggregates (Fig. 2*F*). Importantly, here once again we observed that protein depletion of Sac3 or ArPIKfyve prominently affected the aggregation propensity of Sph1, nearly doubling the proportion of cells with multiple small Sph1-GFP aggregates (Fig. 2, *F–H*, and data not shown). Collectively, these data demonstrate that the reduction of the ArPIKfyve-Sac3 complex in either primary mouse neurons or human neuroblastoma cell line recapitulates the increased aggregation of Sph1 as observed in HEK293 cells. Our data further suggest that in physiological contexts the interaction between ArPIKfyve-Sac3 and Sph1 may stabilize Sph1, preventing its aggregation.

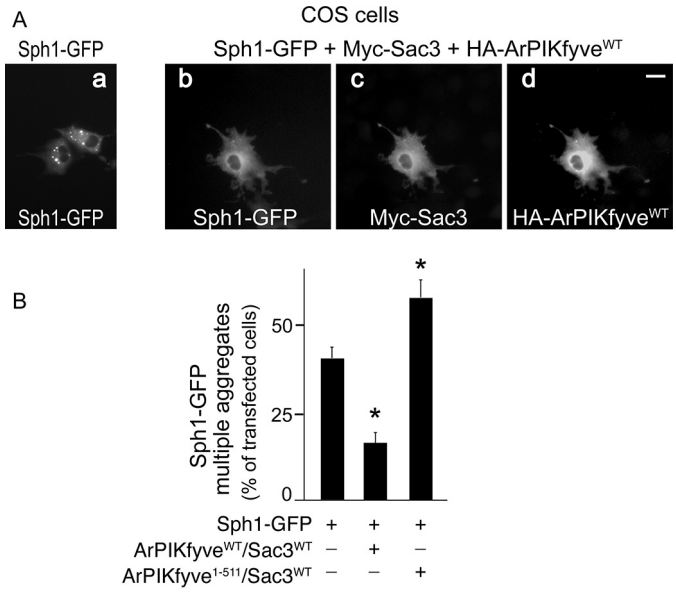

FIGURE 3. **Co-expression of Sac3 with ArPIKfyve^{WT}, but not with ArPIKfyve mutant unable to bind Sac3, reduces aggregation of Sph1-GFP.** COS7 cells were transfected with Sph1-GFP cDNA alone or together with cDNAs of Myc-Sac3^{WT} and either HA-ArPIKfyve^{WT} or HA-ArPIKfyve-(1–511) as detailed under "Experimental Procedures." On the next day, cells were fixed and immunostained consecutively with anti-Myc and anti-HA antibodies to visualize Myc-Sac3 and HA-ArPIKfyve^{WT} or HA-ArPIKfyve-(1–511) proteins, respectively. *A*, representative images of singly Sph1-GFP-expressing cells with multiple small aggregates (*a*) or a triply Sph1-GFP/Myc-Sac3/HA-ArPIKfyve^{WT} (*b–d*)-expressing cell showing diffuse Sph1-GFP staining. *Bar*, 10 μm. *B*, quantitation of cells with multiple small aggregates of Sph1-GFP by viewing more than 100 GFP-positive cells from at least three random fields from three independent experiments, indicating reduced aggregation only in the presence of coexpressed Myc-Sac3-HA-ArPIKfyve^{WT}. *, $p < 0.05$.

Elevated ArPIKfyve-Sac3 Complex Reduces Aggregation of Sph1 in COS Cells—Having established that ArPIKfyve and Sac3 protein depletion facilitates the aggregation of Sph1-GFP, we examined whether increased levels of the two proteins would have the opposite effect. To simultaneously elevate the three proteins at reasonable cell transfection efficiency, we first conducted experiments in COS7 cells proven prone to multigene expression (1, 2). Similar to HEK293 cells, singly expressed Sph1-GFP in this cell type resulted in the formation of multiple small cytoplasmic aggregates in 40–45% of the transfected cells (Fig. 3). Remarkably, however, when Sph1-GFP was co-transfected with ArPIKfyve and Sac3, the proportion of cells displaying multiple small aggregates of Sph1-GFP markedly diminished. Rather, the majority of the triply transfected cells (~10% efficiency of triple transfections) displayed diffuse cytosolic fluorescence signals of Sph1-GFP (Fig. 3). Notably, if Myc-Sac3 or HA-ArPIKfyve were individually coexpressed with Sph1-GFP, a reduction in the proportion of cells with multiple small aggregates of Sph1-GFP was not apparent (Fig. 3*B*). As discussed below, without ArPIKfyve, Myc-Sac3 expression even increased the aggregation of Sph1-GFP.

To further determine the requirement for ArPIKfyve-Sac3 complex formation in the observed functional effect on Sph1, we performed a similar Sph1-GFP aggregation assay in triply transfected COS7 cells but used instead of HA-ArPIKfyve^{WT} an ArPIKfyve N-terminal fragment spanning residues 1–511. The partial ArPIKfyve-(1–511) protein does not associate with Sac3, as ArPIKfyve and Sac3 bind each other through their C

termini as we established previously (1, 2). Quantitation of three independent transfection experiments revealed that, in contrast to ArPIKfyve^{WT}, coexpression of HA-ArPIKfyve$^{1-511}$ with Myc-Sac3 did not decrease the proportion of cells with Sph1-GFP aggregates; in fact, it even increased it, despite the similar expression levels of Sph1-GFP in both triple transfection conditions (Fig. 3*B*, not shown, and see further). These data indicate that only ArPIKfyve^{WT}, competent in forming a stable complex with coexpressed Sac3, can reduce the aggregation propensity of Sph1-GFP.

Elevated ArPIKfyve-Sac3 Complex Attenuates Sph1 Aggregation in a HEK293 Cell Line—To confirm the above data for another cell type and by an approach amenable to biochemical quantitation, we used our HEK293 stable cell line inducibly expressing HA-ArPIKfyve. As established previously and confirmed here, the induced levels of HA-ArPIKfyve in the iArPIKfyve-HEK cells increased by >10-fold over the endogenous protein, whereas those of Sac3 were elevated by 2-fold (6). To produce commensurate increases in Sac3 levels and, hence, to elevate the ArPIKfyve-Sac3 complex, we coexpressed Myc-Sac3 and inspected the aggregation properties of Sph1-GFP by fluorescent microscopy. Roughly 40–45% of singly Sph1-GFP-transfected ArPIKfyve-HEK cells, both Dox-induced and non-induced, exhibited multiple small aggregates of Sph1-GFP (Fig. 4, *A* and *B*). Notably, similar to the triply transfected COS cells, the proportion of cells with aggregates was markedly diminished in iArPIKfyve-HEK cells if Myc-Sac3 was coexpressed. As illustrated in Fig. 4*A*, the appearance of Sph1-GFP-associated fluorescence was rendered diffuse in the majority of the doubly transfected iArPIKfyve-HEK cells.

To confirm this observation biochemically, we quantified the ratio of soluble *versus* insoluble Sph1-GFP in the presence or absence of coexpressed ArPIKfyve-Sac3. Parallel dishes of Sph1-GFP-transfected ArPIKfyve-HEK cells, with or without Myc-Sac3 co-transfection/ArPIKfyve induction, were treated for 2 min with 0.5% Triton X-100 followed by cell scraping in RIPA buffer (30). As illustrated in Fig. 4*C*, whereas Sph1-GFP levels in the total fraction were comparable in the singly and triply expressing cells, they decreased in the Triton-insoluble fraction and slightly increased in the soluble fraction if cells coexpressed HA-ArPIKfyve and Myc-Sac3 (Fig. 4*D*). Together, these data indicate that the ArPIKfyve-Sac3 complex causes a sustained reduction of Sph1 aggregation by increasing Sph1 partitioning into the cytosol.

Elevated ArPIKfyve-Sac3 Protein Complex Fails to Alter the Aggregation of GFAP—The fact that the ArPIKfyve-Sac3 complex interacts with Sph1 suggests that it modulates the aggregation properties of Sph1 in a specific manner. To support this conclusion further, we used a different aggregation-prone protein, GFAP, linked to a neurological condition known as Alexander disease (43). Like Sph1, in disease or upon heterologous expression in mammalian cells, GFAP forms multiple small cytoplasmic aggregates (44). This observation was confirmed herein for GFP-GFAP-transfected COS7 (Fig. 5*A*) and ArPIKfyve-HEK cells (Fig. 5*C*), where we documented multiple small aggregates in ~85% of the GFP-GFAP-transfected cells with or without ArPIKfyve coexpression (Fig. 5, *B* and *D*). However, in contrast to Sph1-GFP, coexpression of ArPIKfyve and Sac3 in

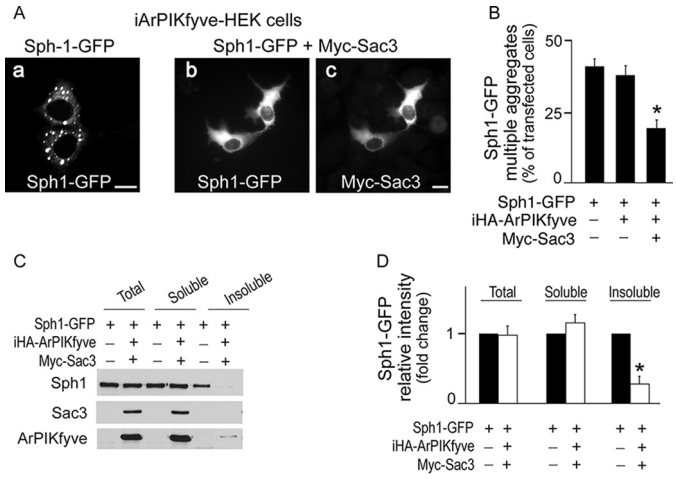

FIGURE 4. **Elevation of ArPIKfyve-Sac3 complex decreases aggregation of Sph1-GFP in ArPIKfyve-HEK cells.** ArPIKfyve-HEK cells were transfected with cDNA of Sph1-GFP alone or together with that of Myc-Sac3 when HA-ArPIKfyve expression was induced (*i*) or not induced. On the next day cells were either processed for immunofluorescence microscopy (*A* and *B*) or underwent protein fractionation to obtain total protein, Triton X-100-soluble, and Triton X-100-insoluble fractions (*C* and *D*) as detailed under "Experimental Procedures." *A*, following fixation and permeabilization, cells were stained with anti-Myc and observed by immunofluorescence microscopy. Shown are typical images of cells with multiple small aggregates by single expression of Sph1-GFP (*a*) or with diffuse distribution of Sph1-GFP if Myc-Sac3 and HA-ArPIKfyve were coexpressed (*b* and *c*). *Bar*, 10 μm. *B*, quantitation of Sph1-GFP aggregates under these conditions, presented as a percentage of cells with multiple cytoplasmic aggregates as determined by viewing more than 100 GFP-positive cells from at least three random fields/condition. *, different *versus* singly Sph1-GFP-transfected cells, $p < 0.05$. Note that expression of HA-ArPIKfyve alone did not significantly alter the percentage of cells with multiple aggregates of Sph1-GFP. *C*, transfected ArPIKfyve-HEK cells were treated with Triton X-100 in PBS to extract the soluble proteins and then scraped in RIPA$^+$ buffer + 0.1% SDS to collect the insoluble proteins. Cells from a duplicate dish were scraped in RIPA$^+$/0.1% SDS to recover total proteins. Equal volumes of the respective fractions were analyzed by Western blotting. Shown are chemiluminescence detections of representative blots illustrating that the partitioning of Sph1-GFP in the insoluble fraction was diminished when coexpressed with Myc-Sac3 and HA-ArPIKfyve. Note that levels of total Sph1-GFP were identical between the singly and triply expressing cells. *D*, relative quantitation by densitometry from three separate Western blots with similar results. *, $p < 0.05$.

these cells by transfections and induction did not alter the aggregation properties of GFP-GFAP, as evidenced by the sustained appearance of multiple small aggregates of GFP-GFAP in the triply expressing COS7 or iArPIKfyve-HEK cells (Fig. 5). Together, these data indicate that increased expression levels of ArPIKyve-Sac3 selectively reduce the aggregation properties of Sph1-GFP.

ArPIKfyve-Sac3 Complex Attenuates Aggresome Formation of Sph1 under Proteasome Inhibition—To reveal the cellular mechanism(s) by which the ArPIKfyve-Sac3 complex leads to reduced aggregation of Sph1, we used a pharmacological approach. Previous studies have established that in HEK293 cells, Sph1-GFP is degraded by the ubiquitin-proteasome system (45, 46). Therefore, we surmised that our observation for down-regulated aggregation of Sph1-GFP could result, in part, by facilitated Sph1 recruitment for clearance by the proteasome in a manner directly or indirectly dependent on its interaction with the ArPIKfyve-Sac3 complex. To address this potential mechanism, we used the aldehyde peptide MG132, a well characterized inhibitor of the 26 S proteasome, aiming at suppressing Sph1 clearance. Such a treatment in HEK293 cells has been

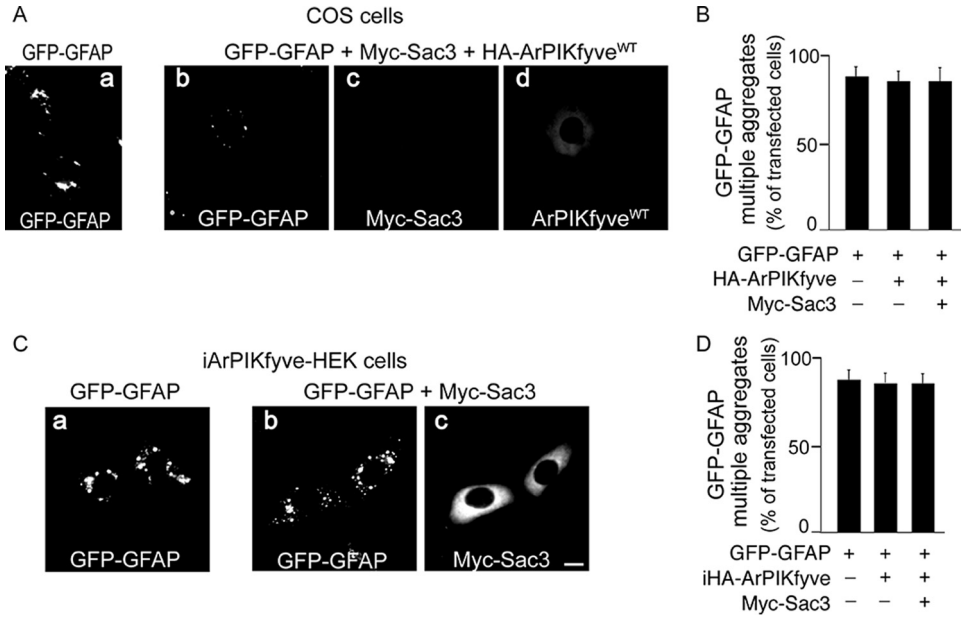

FIGURE 5. **Elevation of ArPIKfyve-Sac3 complex fails to alter aggregation of GFP-GFAP.** *A* and *B*, COS7 cells were transfected with cDNA of GFP-GFAP alone (*a*), in a double combination with cDNA of HA-ArPIKfyve or in a triple combination with cDNAs of HA-ArPIKfyve and Myc-Sac3 (*b–d*). Twenty-four h post-transfection, cells were fixed and processed for immunofluorescence microscopy as detailed under "Experimental Procedures." Shown are representative cells with multiple small aggregates of GFP-GFAP in singly transfected cells (*a*) which persisted in triply transfected cells (*b–d*), whereas Myc-Sac3 (*c*) and HA-ArPIKfyve (*d*) remained diffuse, and quantitative analysis (*B*) of fluorescence microscopy images by monitoring >100 cells/condition in random fields in two separate experiments. *C* and *D*, ArPIKfyve-HEK cells were transfected with GFP-GFAP cDNA alone (*a*) or together with Myc-Sac3 cDNA in the presence of HA-ArPIKfyve induction (*i*) (*b* and *d*). Note the presence of GFP-GFAP aggregates (*b*), despite overexpression of Myc-Sac3 and HA-ArPIKfyve in the iArPIKfyve-HEK cells (*c*). Quantitative analysis (*D*) of fluorescence microscopy images by monitoring >100 cells/condition on random fields in two separate experiments. *Bar*, 10 μm.

shown to result in the formation of a single perinuclear aggresome of Sph1-GFP, resembling Lewy body cytoplasmic inclusions, in a manner independent of Sph1 expression levels but dependent on an intact microtubule network (38, 39, 45). Accordingly, our fluorescence microscopy analyses in MG132-treated triply transfected COS7 cells also revealed aggresome formation in ~80% of the Sph1-GFP transfected cells, occurring in a microtubule-dependent manner (Fig. 6, *A* and *B*, and not shown). Remarkably, co-expression of ArPIKfyve-Sac3 markedly reduced the proportion of cells displaying a single Sph1-GFP-positive aggresome (Fig. 6, *A* and *B*). Rather, in the triply transfected cells we observed predominantly diffuse fluorescence signals of Sph1-GFP, indicative of cytosolic distribution (Fig. 6*A*). Consistently, MG132 treatment in iArPIKfyve-HEK cells co-expressing Myc-Sac3 and Sph1-GFP yielded analogous results (Fig. 6*C*), suggesting the general significance of ArPIKfyve-Sac3-dependent suppression of aggresome formation by Sph1-GFP upon proteolytic inhibition. Together, these data corroborate the conclusion that accelerated proteasomal degradation does not underlie the observed reduction in aggregation/aggresome formation of Sph1-GFP in the presence of overexpressed ArPIKfyve-Sac3.

If ectopically expressed Sac3 is not stabilized through binding to ArPIKfyve, it is quickly degraded by the proteasome (6). Intriguingly, analogous to Sph1-GFP, we observed here that proteasome inhibition by MG132 in both transfected COS7 (Fig. 6*A*, *c*, *arrow*) and HEK293 cells (Fig. 6*D*) also triggered the recruitment of ectopically expressed Sac3 to the aggresome observed in ~70% of the transfected cells. The aggresome formation of HA-Sac3 was verified by the requirement for an intact microtubule network (Fig. 6*D*, *b*). Remarkably, if cells were concurrently co-transfected with Myc-ArPIKfyve and HA-Sac3, MG132 failed to form HA-Sac3-positive aggresomes in practically all of the doubly transfected HEK293 cells (Fig. 6, *D* and *E*). Rather, the immunofluorescence signals of HA-Sac3 and, hence, Myc-ArPIKfyve were diffuse, indicative of a cytosolic distribution. Likewise, whereas ~10% of the singly transfected cells also formed multiple small aggregates of HA-Sac3 under proteasome inhibition (Fig. 6*E*), this number was reduced down to ~1% if the HA-Sac3-expressing cells coexpressed Myc-ArPIKfyve (Fig. 6*E*). These data suggest that upon ArPIKfyve binding, Sac3 is solubilized and that, once formed, the complex is kept stable in the cytosol, preventing aggregation and aggresome formation of Sac3 under proteasome inhibition.

ArPIKfyve-Sac3 Complex Fails to Reduce Aggregation of Sph1-GFP under Arrested Basal Autophagy—Another mechanism by which the ArPIKfyve-Sac3 complex may reduce aggregates of Sph1-GFP is through the acceleration of autolysosomal clearance. The rationale for this prediction stems from findings for the removal of Sph1 aggregates by constitutive autophagy in SH-SY5Y cells (42) and for arrested autophagic progression in Sac3-deficient cells (7). Moreover, the ArPIKfyve-Sac3 complex, alone or with PIKfyve, has been reported to be essential for the proper performance of the endolysosomal system (5). To this end, we inhibited basal autophagy with 3-MA, which blocks the activity of Vps34, a key player in autophagosome formation (47). 3-MA-treatment of Sph1-GFP-transfected ArPIKfyve-HEK cells in serum-containing media resulted in profound increases in the proportion of cells with Sph1-GFP aggregates,

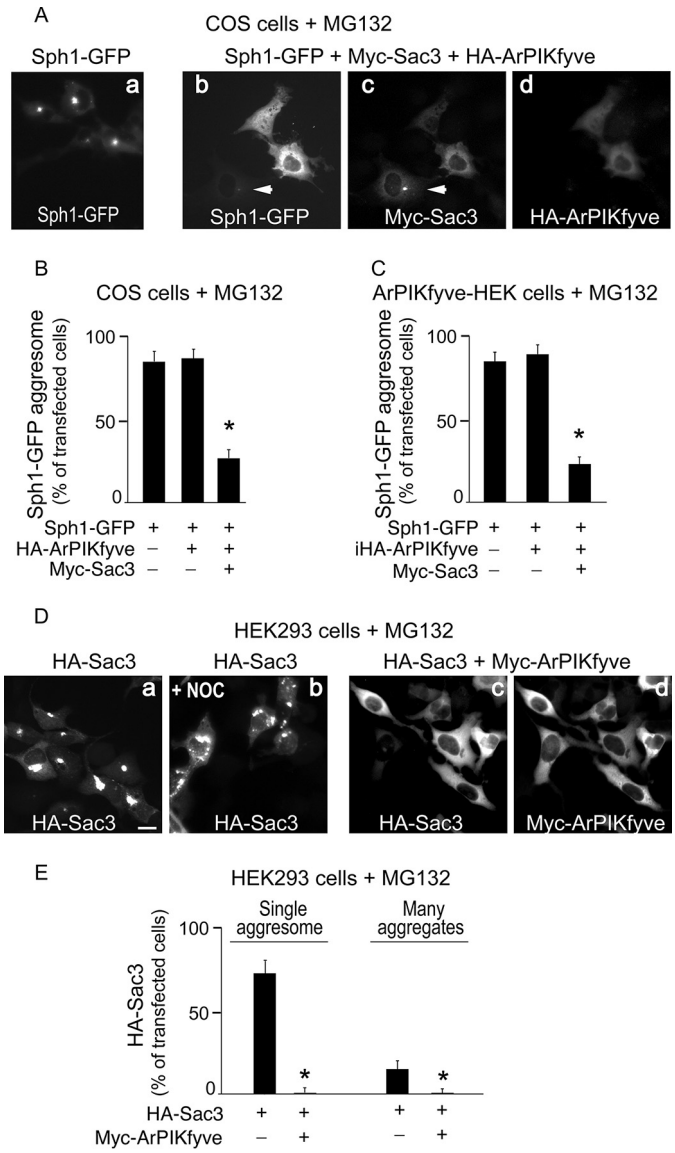

FIGURE 6. **Aggresome formation of Sph1-GFP under proteasome inhibition is reduced by elevation of ArPIKfyve-Sac3.** *A* and *B*, 24 h post-transfection with the indicated cDNAs, COS7 cells were treated with MG132 (5 μM) for 5 h, fixed, and processed for immunofluorescence microscopy. *A*, representative images illustrating the appearance of large single perinuclear aggresomes independent of the expression level of singly transfected Sph1-GFP (*a*) and the typical diffuse appearance of Sph1-GFP (*b*) in the presence of Myc-Sac3 (*c*) and HA-ArPIKfyve (*d*) in triply transfected cells. *Arrowheads* in *b* and *c* point to the aggresome formed when Myc-Sac3 is expressed without HA-ArPIKfyve. *B*, percentage of cells with Sph1-GFP aggresomes from three separate experiments. Note that HA-ArPIKfyve alone does not affect Sph1-GFP aggresome formation. *, $p < 0.05$. *C*, HA-ArPIKfyve-HEK cells were transfected with cDNA of Sph1-GFP alone or with cDNA of Myc-Sac3 in the presence or absence of induced HA-ArPIKfyve expression. Twenty-four h later, cells were treated with MG132 (5 μM) for 5 h and then processed for immunofluorescence microscopy. Shown is quantitation of cells with a single aggresome presented as the percentage of transfected Sph1-GFP. *, $p < 0.05$. *D* and *E*, aggresome formation of HA-Sac3 under proteasome inhibition is reduced by elevation of ArPIKfyve. *D*, HEK293 cells were transfected with cDNA of HA-Sac3 alone (*a* and *b*) or together with Myc-ArPIKfyve cDNA (*c* and *d*). Twenty-four h post-transfection cells were treated with MG132 (5 μM) for 5 h in the presence or absence of nocodazole (*NOC*, 5 μM) as indicated. Note the reduced aggresome formation and the diffuse distribution of HA-Sac3 by co-expression of Myc-ArPIKfyve (*c* and *d*). *Bar*, 10 μm. *E*, quantitation of the proportion of transfected cells with a single aggresome or multiple aggregates of HA-Sac3 and the fold decrease by Myc-ArPIKfyve. *, different *versus* single HA-Sac3 transfection ($p < 0.05$).

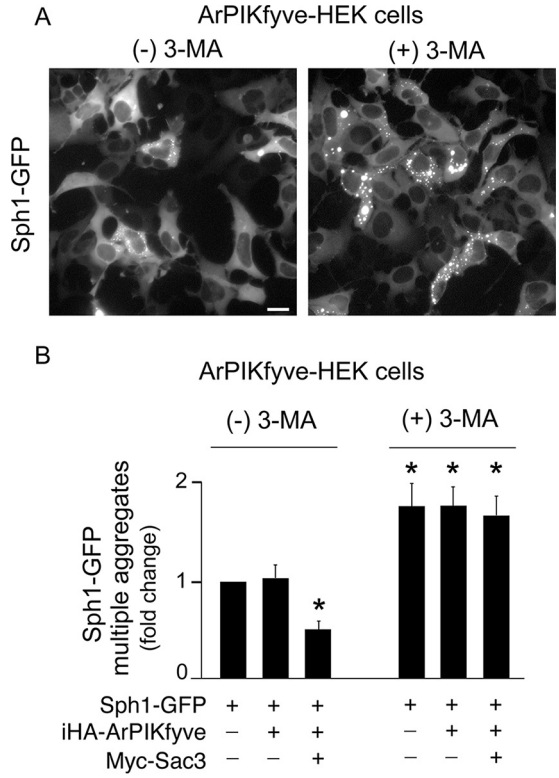

FIGURE 7. **Elevation of ArPIKfyve-Sac3 complex fails to reduce aggregation of Sph1-GFP under inhibition of basal autophagy.** ArPIKfyve-HEK cells were transfected with cDNA of Sph1-GFP alone or together with that of Myc-Sac3 and then induced (*i*) or not induced to express HA-ArPIKfyve as indicated. Twenty-four h later, cells were treated without or with 3-MA (10 mM) in a complete 10% FBS-containing medium. Twenty-four h post-treatment, cells were fixed and processed for fluorescence/immunofluorescence microscopy with the anti-Myc/Alexa Fluor 568 anti-mouse as primary/secondary antibody as described under "Experimental Procedures." Representative fluorescence images of singly expressed Sph1-GFP with and without 3-MA treatment show the significantly increased proportion of cells with multiple aggregates by 3-MA (*A*), and the relative fold change in the number of Sph1-GFP-transfected cells containing multiple small aggregates upon treatment with 3-MA under different conditions is quantitated (*B*). Quantitation is based on counting >100 cells/condition in three separate experiments. *, different *versus* single Sph1-GFP transfection without 3-MA ($p < 0.05$). *Bar*, 10 μm.

consistent with their arrested clearance through basal quality control autophagy (Fig. 7). Intriguingly, however, coexpression of Sac3 and ArPIKfyve did not ameliorate the aggregation of Sph1-GFP in the presence of 3-MA inhibition (Fig. 7*B*). Because Vps34-synthesized PtdIns3P serves as a main substrate for PtdIns(3,5)P_2 production by PIKfyve (48), 3-MA may potentially affect Sac3 phosphatase functionality in a manner unrelated to basal autophagy. However, we observed a similar inability of expressed ArPIKfyve-Sac3 to reduce Sph1-GFP aggregation in iArPIKfyve-HEK cells upon inhibiting basal autophagy by chloroquine, a compound that acts in a Vps34-unrelated manner (data not shown). These data corroborate the notion that ArPIKfyve-Sac3 complex directly or indirectly facilitates the clearance of Sph1 aggregates through constitutive autophagy.

ArPIKfyve-Sac3-dependent Attenuation of Aggregation by Sph1-GFP Requires Active Sac3 Phosphatase—To gain further mechanistic insights as to whether the observed ArPIKfyve-Sac3-dependent attenuation in aggregation propensity of

Sph1-GFP is related to Sac3 phosphatase activity, we used a phosphatase-deficient point mutant, Sac3^{D488A}, carrying a substitution within the active site. As we had established previously, this substitution does not alter the ability of Sac3^{D488A} to bind ArPIKfyve (1–3). To this end, we coexpressed Sph1-GFP with HA-Sac3^{D488A} or HA-Sac3^{WT} in iArPIKfyve-HEK cells and monitored the aggregation of Sph1-GFP by fluorescence microscopy. Detection of Sac3 proteins was achieved with affinity-purified anti-Sac3 antibodies (3), as the HA-tag was also present in ArPIKfyve. Remarkably, we observed significant differences in the proportion of cells with aggregates of Sph1-GFP dependent on the presence or absence of Sac3 phosphatase activity. Thus, unlike with HA-Sac3^{WT}, in the presence of iArPIKfyve the aggregation potential of Sph1-GFP was not reduced by coexpressed HA-Sac3^{D488A}, despite the diffuse cytosolic distribution of the latter, indicative of binding to and solubilization by ArPIKfyve (Fig. 8*A*). Likewise, aggresome formation of Sph1-GFP upon proteolytic stress was not attenuated if the phosphatase-inactive Sac3^{D488A} was present instead of Sac3^{WT} (not shown). These data suggest that the effect of ArPIKfyve-Sac3 in reducing aggregation of Sph1-GFP proceeds in a manner dependent on Sac3 phosphatase activity.

Coexpressed Sph1 and Sac3 Potentiate each Other's Aggregation in a Manner Reversible by ArPIKfyve—While conducting pairwise protein overexpression, we noted that in the absence of ArPIKfyve, Myc-Sac3 augmented cytoplasmic inclusion formation by Sph1-GFP (Figs. 3*B* and 6*A*, *c*). This observation, coupled with the documented presence of both Sac3 and Sph1 in Lewy bodies in patients with Lewy body dementia pathologies and α-synucleinopathies (49, 50), prompted us to scrutinize the inclusion formation upon binary expression of Sac3 and Sph1. We used Sph1-GFP and Myc-Sac3, which, as indicated above, when expressed individually, formed multiple small aggregates in ~45 and 10%, respectively, of the transfected ArPIKfyve-HEK cells. Intriguingly, coexpression of Sph1-GFP with Myc-Sac3 resulted in a markedly greater proportion of cells with aggregates of Sph1, reaching as high as 80–85% of the doubly transfected cells at 24–48 h post-transfection (Fig. 9*A*). The proportion of cells with multiple Myc-Sac3-positive aggregates was also profoundly increased (>3-fold) in the presence of Sph1-GFP coexpression (Fig. 9*B*). Confocal microscopy examination of the doubly transfected cells visualized individual Myc-Sac3 or Sph1-GFP-positive aggregates (Fig. 9*C*, *a–c*), consistent with the lack of physical interaction between Sph1 and Sac3. However, in some cells, we saw aggregates positive for both proteins to coalesce (Fig. 9*C*, *d–f*) or Myc-Sac3 fluorescence signals to surround the foci of Sph1-GFP fluorescence (Fig. 9*C*, *g–i*).

To determine whether these aggregates could still be dispersed by ArPIKfyve overexpression, at 24 h post-Myc-Sac3/Sph1-GFP transfection, ArPIKfyve-HEK cells were induced to express ArPIKfyve. Remarkably, we observed profound decreases in the proportion of cells with Myc-Sac3 and Sph1-GFP aggregates upon overexpression of ArPIKfyve (Fig. 9, *A* and *B*). Concordantly, biochemical analyses indicated significant levels of Myc-Sac3 and Sph1-GFP in the Triton-insoluble fraction, both of which decreased subsequent to ArPIKfyve expression (Fig. 9*D*). Together, these data demonstrate that the

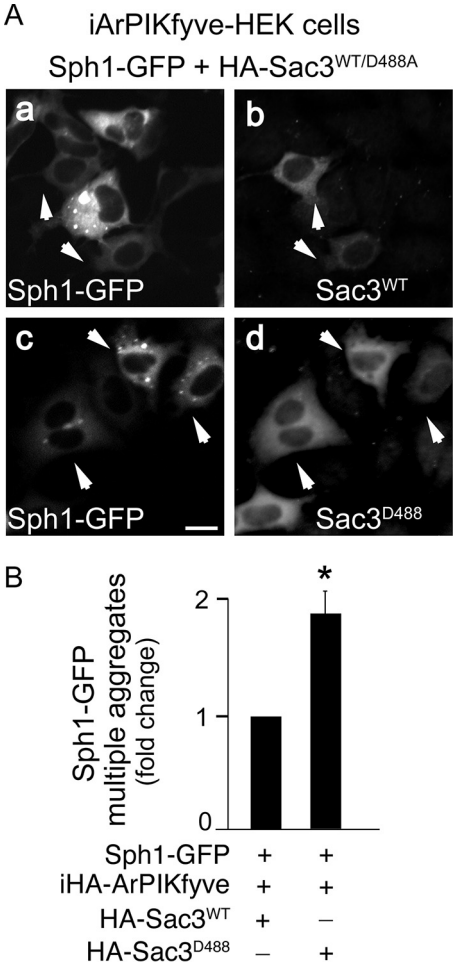

FIGURE 8. **Reduced aggregation of Sph1-GFP by ArPIKfyve-Sac3 requires active Sac3 phosphatase.** ArPIKfyve-HEK cells were co-transfected with cDNAs of Sph1-GFP and either HA-Sac3^{WT} or the phosphatase inactive mutant HA-Sac3^{D488A} when ArPIKfyve expression was induced (*i*). On the next day, iArPIKfyve-HEK cells were fixed, permeabilized, and stained with affinity-purified anti-Sac3 antibodies and CY3-conjugated anti-rabbit secondary antibody as described under "Experimental Procedures." *A*, shown are representative images of iArPIKfyve-HEK cells co-transfected with HA-Sac3^{WT} and Sph1-GFP (*a* and *b*) or co-transfected with HA-Sac3^{D488A} and Sph1-GFP (*c* and *d*). Note the diffuse Sph1-GFP distribution with coexpressed HA-Sac3^{WT} but multiple small aggregates with coexpressed HA-Sac3^{D488A} (*arrowheads*). *Bar*, 10 μm. *B*, the proportion of Sac3^{WT}/Sac3^{D488A}-positive cells with multiple small Sph1^{WT}-GFP aggregates was determined by counting >100 doubly transfected cells from random fields per condition from three separate experiments, and presented as the relative fold difference. *, $p < 0.05$.

presence of aggregates of Sph1 instigates Sac3 aggregation, and vice versa, that high levels of aggregated Sac3 promote Sph1 aggregation. Significantly, these data indicate that once formed, Sph1 or Sac3 aggregates could be dissociated by overexpression of ArPIKfyve.

The ability of the Sac3-ArPIKfyve complex to disintegrate already formed Sph1 aggregates was also verified by another approach in which parallel dishes of the ArPIKfyve-HEK cell line were first transfected with Sph1-GFP and 24 h later were transfected/induced to express the Myc-Sac3/HA-ArPIKfyve. The results from these experiments also demonstrated a small but statistically significant reduction (~20% decrease, $p < 0.05$) in the proportion of cells with aggregates of Sph1-GFP. Notably, cells with Myc-Sac3 aggregates were only rarely seen under these conditions, consistent with Myc-Sac3 solubilization upon

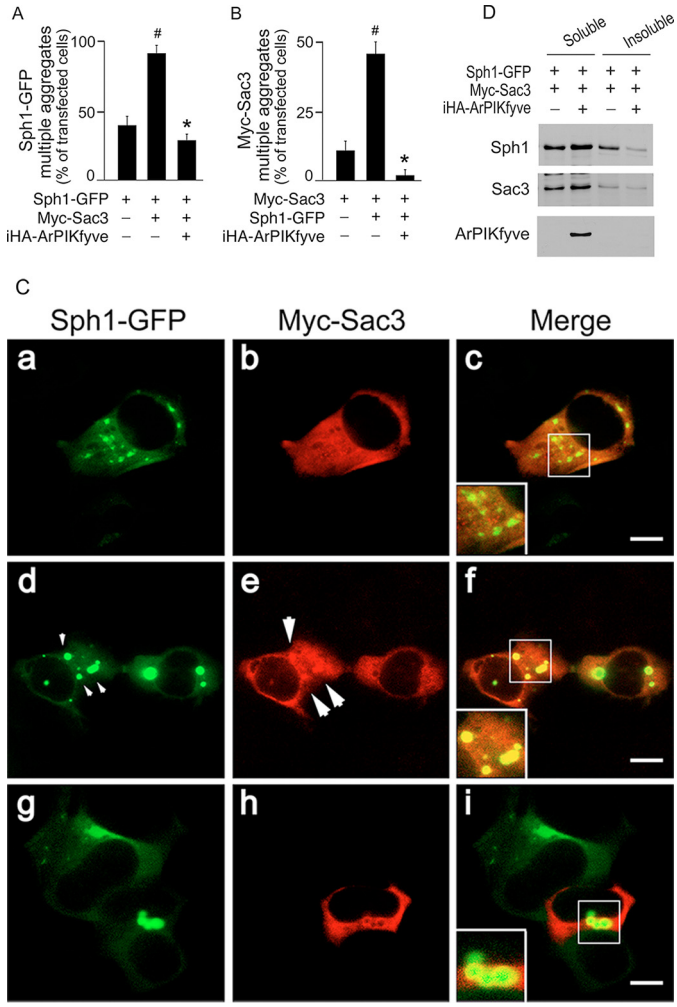

FIGURE 9. **Coexpressed Sph1 and Sac3 potentiate each other's aggregation in a manner reversible by ArPIKfyve.** ArPIKfyve-HEK cells were co-transfected with cDNAs of Sph1-GFP and Myc-Sac3. Twenty-four h post-transfection, HA-ArPIKfyve expression was induced where indicated. On the next day cells were processed for fluorescence microscopy (*A–C*) or underwent protein fractionation to obtain Triton X-100-soluble and -insoluble fractions (*D*) as detailed under "Experimental Procedures." *A* and *B*, quantitation of the fluorescence microscopy indicating the percentage of cells with multiple aggregates of Sph1-GFP and/or Myc-Sac3 determined by viewing >100 doubly transfected cells/condition in three separate experiments. Note the marked increase of cells with multiple aggregates of Sph1-GFP and Myc-Sac3 in the co-transfected cells (#, different *versus* singly transfected cells, $p < 0.05$) and the significant diminution of aggregates by both proteins upon ArPIKfyve expression (*, different *versus* singly and doubly transfected cells, $p < 0.05$). *C*, confocal microscopy of co-transfected Sph1-GFP/Myc-Sac3 non-induced cells performed as detailed under "Experimental Procedures." Representative images illustrating three typical observations: *a–c*, individual Sph1-GFP-positive small aggregates with no colocalization with Myc-Sac3 as apparent by the *green* aggregates in the *merged images* and *inset* in *c*. *d–f*, coalescence of some aggregates formed by Sph1-GFP (*d*, *small arrowheads*) and Myc-Sac3 (*e*, *arrowheads*) as apparent by the yellow aggregates in the *merged image* and *inset* in *f*. *g–i*, Myc-Sac3 inclusions forming rings surrounding aggregates by Sph1-GFP as evident by the presence of *yellow* as well as separate *green* and *red* in the *merged image* and *inset* in *i*. *Bar*, 10 μm. *D*, cells were treated with Triton X-100 to extract the soluble proteins and then scraped in $RIPA^+$/0.1% SDS to collect the insoluble proteins. An equal volume of the respective fraction was analyzed by Western blotting. Shown are chemiluminescence detections of representative blots illustrating that HA-ArPIKfyve expression diminished Sph1-GFP and Myc-Sac3 levels in the Triton X-100-insoluble fraction but increased these levels in the Triton X-100-soluble fraction.

concurrent expression of ArPIKfyve. Together, these data further indicate that even when formed, a subpopulation of aggregates of Sph1 is competent for solubilization and removal by the ArPIKfyve-Sac3 complex.

Discussion

Cytoplasmic aggregates and inclusions are pathological hallmarks of a number of neurodegenerative diseases, including Parkinson disease, in which the presence of α-Syn inclusions is associated with the onset and progression of the disease (51–53). Studies in cell systems have established that α-Syn aggregation is potentiated through interaction with Sph1 (23, 50, 54). Concordantly, post mortem brain examinations have demonstrated that both Sph1 and α-Syn are major molecular components of Lewy bodies found in α-synucleinopathies (25, 50). In this study, we identified for the first time that Sph1 interacts with the heterodimeric complex that comprises PtdIns(3,5)P_2 5-phosphatase Sac3 and the scaffolding protein ArPIKfyve in both neuronal and non-neuronal cells (Fig. 1, *A* and *B*). The interaction is most likely direct, as judged by the ability of immunopurified Sph1-Myc to capture specifically the purified ArPIKfyve-Sac3 complex produced by a baculovirus expression system (Fig. 1*C*). By biochemical and/or morphological approaches in HEK293, COS, and SH-SY5Y cell lines or primary mouse cortical neurons, we further showed that protein knockdown of ArPIKfyve, Sac3, or both increased the proportion of cells with multiple aggregates of Sph1-GFP (Fig. 2), whereas elevated ArPIKfyve-Sac3 complex reduced aggregate formation, increasing the soluble form of Sph1-GFP (Figs. 3 and 4). Notably, whereas both Sph1-GFP and GFP-GFAP are aggregation-prone proteins, ArPIKfyve-Sac3-dependent reduction in aggregation was observed only for Sph1-GFP but not for GFP-GFAP (Figs. 3–5), underscoring the specificity of the Sph1 physical interaction with the ArPIKfyve-Sac3 complex in this effect. Importantly, the response to proteolytic stress that triggers coalescence of multiple small aggregates of Sph1-GFP into a single aggresome in a manner unrelated to protein expression levels (39) was also attenuated if the ArPIKfyve-Sac3 complex was coexpressed (Fig. 6). By contrast, the ArPIKfyve-Sac3 complex was largely ineffective in reducing aggregation of Sph1 if constitutive autophagy was inhibited (Fig. 7). These data are consistent with the notion that ArPIKfyve-Sac3 reduces aggregation of Sph1-GFP through several mechanisms: first, by stabilization of Sph1 in the cytosol through formation of a soluble ArPIKfyve-Sac3-Sph1 complex; second, by recruitment of aggregated Sph1 by cytosolic ArPIKfyve-Sac3; and third, by removal of Sph1 aggregates via basal quality control autophagy. The proposed model is presented in Fig. 10.

An important insight in our study is that the Sac3-ArPIKfyve-dependent reduction of aggregates formed by Sph1 requires active Sac3 phosphatase activity. This conclusion was based on our finding for the inability of the phosphatase-deficient point mutant $Sac3^{D488}$, carrying substitution in the conserved signature motif $C(X)_5R(S/T)$ of the Sac3 active site, to elicit this effect (Fig. 8), despite intact binding to ArPIKfyve (2). Whereas defective phosphoinositide metabolism as causative in Parkinsonism is elusive, its potential role is suggested by the fact that two hereditary disease-related proteins, *i.e.* PARK6 and PARK20, are linked with the 3- and 5-phosphoinositide phosphatase activities of *PTEN* and *SNJ1*, respectively, both of which also harbor the signature $C(X)_5R(S/T)$ motif (55, 56).

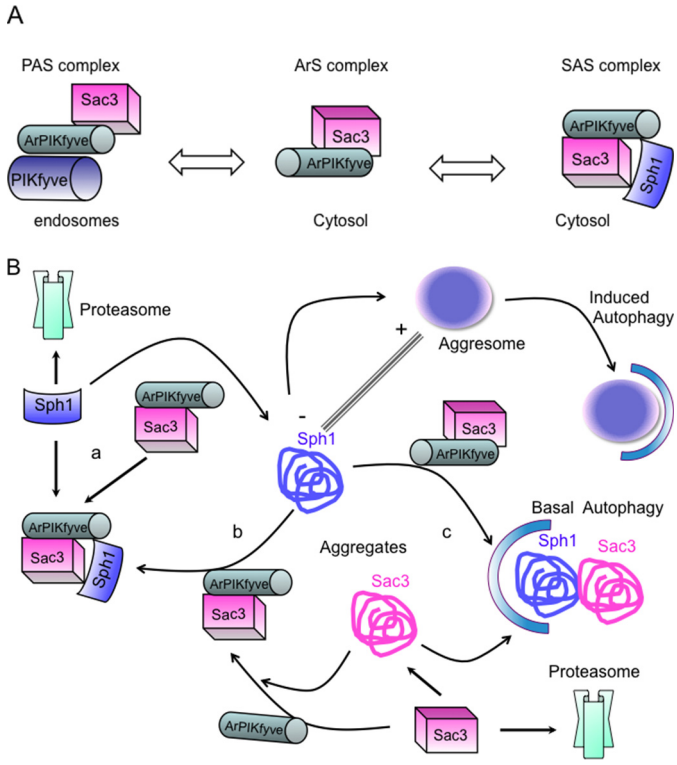

FIGURE 10. **Functional significance of the ArPIKfyve-Sac3 complex interactions.** *A*, Sac3 is stabilized in the cytosol by binding ArPIKfyve and forming the ArPIKfyve-Sac3 (ArS) complex (6). A subfraction of the cytosolic ArPIKfyve-Sac3 complex is recruited to endosomal membranes where it interacts with PIKfyve (PAS) to facilitate the synthesis and turnover of PtdIns(3,5)P_2 (1, 2) or forms a triple complex with Sph1 in the cytosol (*SAS*, Sac3-ArPIKfyve-Sph1; this study). *B*, proposed mechanisms by which the ArS complex reduces aggregate formation by Sph1. Through direct physical interaction, ArPIKfyve stabilizes and solubilizes Sac3, which prevents Sac3 proteasome degradation and aggregation. The ArS complex interacts with Sph1 in the cytosol preventing misfolding, aggregation, and aggresome formation upon proteolytic stress of Sph1 (*a*). Formation of multiple small aggregates of Sph1 is attenuated upon interaction with the ArS complex and the formation of a soluble SAS complex (*b*) or by clearance through constitutive autophagy facilitated by the ArS complex (*c*). A single large aggresome of Sph1 formed by proteasome inhibition can be removed by induced autophagy (42). The effect of the ArS complex in this step has not been examined.

Reported alterations in mouse models with *Pten*-deficient dopaminergic neurons also corroborate the role of phosphoinositides (57). Furthermore, the central region of Sph1, which encompasses ankyrin repeats and the coiled-coil domain, is required for the formation of both multiple small aggregates in basal conditions and a single aggresome upon proteasome inhibition (39). Although our study did not pinpoint the domain interactions, we speculate that the binding between the ArPIKfyve-Sac3 complex and Sph1 engages this central region of the Sph1 molecule. It is conceivable that by shielding the hydrophobic domains, ArPIKfyve-Sac3 stabilizes the Sph1-GFP protein in the cytosol, thereby diminishing its aggregation propensity and aggresome formation upon proteolytic stress (Fig. 6). It will be important in future studies to clarify details about the relationship between the aggregation properties of Sph1 and PtdIns(3,5)P_2/PtdIns5P turnover as well as the domain interactions.

One particularly important observation in our study was the ability of the expressed ArPIKfyve-Sac3 complex to disperse already formed multiple aggregates of Sph1-GFP, which was apparent if the basal autophagy was intact. This effect was prominent under the setting of marked increases of Sph1-GFP aggregation if coexpressed with Sac3 in the absence of ArPIKfyve. Under these conditions, we observed an increased aggregation propensity not only of Sph1 but also of Sac3 (Fig. 9), likely due to the molecularly crowded environment created by the excessive accumulation of the aggregation-prone proteins, whereby aggregates of Sph1 may act as a seed for Sac3 aggregation. Notably, overexpressed ArPIKfyve alone did not alter the aggregation propensity of Sph1-GFP, whereas it reduced that of Sac3 (Figs. 4, 6, and 9), likely due to the binding and stabilizing of Sac3 in the cytosol. These data suggest that in the presence of aggregates by both Sac3 and Sph1, the observed reduced aggregation properties of Sph1-GFP upon ArPIKfyve coexpression is secondary to Sac3 shifting from a form of multiple small aggregates to a soluble complex with ArPIKfyve (Fig. 10). These findings and considerations further substantiate our conclusion that the elevated ArPIKfyve-Sac3 complex not only prevents the formation but also promotes the breakdown of already formed aggregates by Sph1-GFP (Fig. 10).

That excessive levels of Sac3 and Sph1 can instigate profound protein aggregation is particularly intriguing in light of recent immunofluorescence microscopy studies documenting Sac3 together with α-Syn in Lewy bodies in PD and Lewy body dementia patients (49). Notably, in some Sac3/Sph1-coexpressing cells we also observed coalescence of Myc-Sac3 and Sph1-GFP-associated fluorescence within the cytoplasmic inclusions (Fig. 9*C*), implying a potential link of Sac3 with α-Syn. Although *FIG4*/*SAC3* gene amplification or gain-of-function polymorphism in PD has not yet been reported, excessive accumulation of Sac3 protein has been observed recently in triple negative breast cancer cell types (58). These data, together with the evidence that some forms of PD pathology are triggered by multiplication of the *SNCA* gene and/or elevated expression of α-Syn, which increase α-Syn propensity to aggregate (53, 59, 60), make the *FIG4*/*SAC3* genome-wide association study in the PD cases an important objective. The neuropathology in patients with familial Parkinsonism, in addition to a nigral neuronal loss and the presence of widespread Lewy bodies in the brainstem or cerebral cortex, is characterized by vacuolation within the temporal lobe and lower neurons (61–63). Notably, the known *FIG*/*SAC3*-linked neurological disorders in humans or mice (pale tremor mice) are all triggered by Sac3 deficiency and are associated with neuronal vacuolation or the accumulation of electron-dense inclusion bodies in different cell types (5, 9, 14, 15, 40). Consistently, we also observed increased cytoplasmic inclusions of Sph1 upon Sac3 depletion in both neuronal and non-neuronal cells (Fig. 2). Together, the data from our study coupled with those in the literature support the conclusion that both the excessive accumulation and protein deficiency of Sac3 potentiate the aggregation of Sph1, and thus either condition could precipitate the PD onset.

That the ArPIKfyve-Sac3 complex could shift Sph1 distribution from a form of multiple aggregates toward the soluble form suggests potential therapeutic potential for this phenomenon. Whereas inclusion formation is considered a common pathological hallmark of many neurodegenerative disorders, views on whether inclusions are neuroprotective or toxic are discordant

(51). In regard to aggregation by α-Syn/Sph1, the majority of studies in cell or mouse models support the view that the aggregates are toxic (64–70). Future attempts to block aggregate formation or to break down formed aggregates of Sph1 based on the ArPIKfyve-Sac3 complex may prove beneficial as a therapeutic approach to reducing neurodegeneration in PD. In any case, the current study provides new insights and important clues about the molecular means for reducing cytoplasmic aggregates formed by Sph1 or Sac3.

Author Contributions—O. C. I. performed microscopy analyses and prepared the figures for these analyses, and X. C. performed the mass spectrometry, bioinformatics, and drafted the pertinent sections. D. S. generated HEK293 stable cell line (23L), performed the Western blotting assays, and prepared the figures of these analyses; L. M. C. provided technical assistance in cell transfections and antibody testing; R. K. provided expertise in primary cortical neuron culturing; and E. J. T. participated in data analyses. O. C. I., X. C., and A. S. interpreted the data, and A. S. and O. C. I. conceived the experiments. A. S. coordinated the study and drafted the manuscript, which was edited and revised by O. C. I. All authors reviewed the results and approved the final version of the manuscript.

Acknowledgments—We thank Drs. Virginia Lee, Michael Sherman, and James Goldman for the Synphilin-1 and GFAP constructs and Rochelle LaMacchio for outstanding secretarial assistance. We thank Dr. Joyce Benjamen for providing rat neuron cultures in the initial experiments. The senior author expresses gratitude to the late Violeta Shisheva for her many years of support.

References

1. Sbrissa, D., Ikonomov, O. C., Fenner, H., and Shisheva, A. (2008) ArPIKfyve homomeric and heteromeric interactions scaffold PIKfyve and Sac3 in a complex to promote PIKfyve activity and functionality. *J. Mol. Biol.* **384,** 766–779
2. Ikonomov, O. C., Sbrissa, D., Fenner, H., and Shisheva, A. (2009) PIKfyve-ArPIKfyve-Sac3 core complex: contact sites and their consequence for Sac3 phosphatase activity and endocytic membrane homeostasis. *J. Biol. Chem.* **284,** 35794–35806
3. Sbrissa, D., Ikonomov, O. C., Fu, Z., Ijuin, T., Gruenberg, J., Takenawa, T., and Shisheva, A. (2007) Core protein machinery for mammalian phosphatidylinositol 3,5-bisphosphate synthesis and turnover that regulates the progression of endosomal transport: novel Sac phosphatase joins the ArPIKfyve-PIKfyve complex. *J. Biol. Chem.* **282,** 23878–23891
4. Shisheva, A., Sbrissa, D., and Ikonomov, O. (2015) Plentiful PtdIns5P from scanty PtdIns(3,5)P2 or from ample PtdIns? PIKfyve-dependent models: evidence and speculation (response to: DOI 10.1002/bies.201300012). *Bioessays* **37,** 267–277
5. Shisheva, A. (2012) PIKfyve and its lipid products in health and in sickness. *Curr. Top. Microbiol. Immunol.* **362,** 127–162
6. Ikonomov, O. C., Sbrissa, D., Fligger, J., Delvecchio, K., and Shisheva, A. (2010) ArPIKfyve regulates Sac3 protein abundance and turnover: disruption of the mechanism by Sac3I41T mutation causing Charcot-Marie-Tooth 4J disorder. *J. Biol. Chem.* **285,** 26760–26764
7. Lenk, G. M., and Meisler, M. H. (2014) Mouse models of PI(3,5)P2 deficiency with impaired lysosome function. *Methods Enzymol.* **534,** 245–260
8. Zhang, X., Chow, C. Y., Sahenk, Z., Shy, M. E., Meisler, M. H., and Li, J. (2008) Mutation of *FIG4* causes a rapidly progressive, asymmetric neuronal degeneration. *Brain* **131,** 1990–2001
9. Li, J. (2013) Charcot-Marie-Tooth neuropathy type 4J, in *GeneReviews* (Pagon, R. A., Adam, M. P., Ardinger, H. H., Bird, T. D., Dolan, C. R., Fong, C. T., Smith, R. J. H., and Stephens, K., eds) pp. 169431, University of Washington, Seattle
10. Lenk, G. M., Ferguson, C. J., Chow, C. Y., Jin, N., Jones, J. M., Grant, A. E., Zolov, S. N., Winters, J. J., Giger, R. J., Dowling, J. J., Weisman, L. S., and Meisler, M. H. (2011) Pathogenic mechanism of the *FIG4* mutation responsible for Charcot-Marie-Tooth disease CMT4J. *PLoS Genet.* **7,** e1002104
11. Verdiani, S., Origone, P., Geroldi, A., Bandettini Di Poggio, M., Mantero, V., Bellone, E., Mancardi, G., Caponnetto, C., and Mandich, P. (2013) The *FIG4* gene does not play a major role in causing ALS in Italian patients. *Amyotroph. Lateral Scler. Frontotemporal Degener.* **14,** 228–229
12. Chow, C. Y., Landers, J. E., Bergren, S. K., Sapp, P. C., Grant, A. E., Jones, J. M., Everett, L., Lenk, G. M., McKenna-Yasek, D. M., Weisman, L. S., Figlewicz, D., Brown, R. H., and Meisler, M. H. (2009) Deleterious variants of FIG4, a phosphoinositide phosphatase, in patients with ALS. *Am. J. Hum. Genet.* **84,** 85–88
13. Tsai, C. P., Soong, B. W., Lin, K. P., Tu, P. H., Lin, J. L., and Lee, Y. C. (2011) FUS, TARDBP, and SOD1 mutations in a Taiwanese cohort with familial ALS. *Neurobiol. Aging* **32,** 553.e513–521
14. Campeau, P. M., Lenk, G. M., Lu, J. T., Bae, Y., Burrage, L., Turnpenny, P., Román Corona-Rivera, J., Morandi, L., Mora, M., Reutter, H., Vulto-van Silfhout, A. T., Faivre, L., Haan, E., Gibbs, R. A., Meisler, M. H., and Lee, B. H. (2013) Yunis-Varon syndrome is caused by mutations in *FIG4*, encoding a phosphoinositide phosphatase. *Am. J. Hum. Genet.* **92,** 781–791
15. Nakajima, J., Okamoto, N., Shiraishi, J., Nishimura, G., Nakashima, M., Tsurusaki, Y., Saitsu, H., Kawashima, H., Matsumoto, N., and Miyake, N. (2013) Novel *FIG4* mutations in Yunis-Varon syndrome. *J. Hum. Genet.* **58,** 822–824
16. Baulac, S., Lenk, G. M., Dufresnois, B., Ouled Amar Bencheikh, B., Couarch, P., Renard, J., Larson, P. A., Ferguson, C. J., Noé, E., Poirier, K., Hubans, C., Ferreira, S., Guerrini, R., Ouazzani, R., El Hachimi, K. H., Meisler, M. H., and Leguern, E. (2014) Role of the phosphoinositide phosphatase *FIG4* gene in familial epilepsy with polymicrogyria. *Neurology* **82,** 1068–1075
17. Ikonomov, O. C., Sbrissa, D., Delvecchio, K., Xie, Y., Jin, J. P., Rappolee, D., and Shisheva, A. (2011) The Phosphoinositide Kinase PIKfyve Is vital in early embryonic development: preimplantation lethality of PIKfyve$^{-/-}$ embryos but normality of PIKfyve$^{+/-}$ mice. *J. Biol. Chem.* **286,** 13404–13413
18. Reifler, A., Lenk, G. M., Li, X., Groom, L., Brooks, S. V., Wilson, D., Bowerson, M., Dirksen, R. T., Meisler, M. H., and Dowling, J. J. (2013) Murine Fig4 is dispensable for muscle development but required for muscle function. *Skelet. Muscle* **3,** 21
19. Sbrissa, D., Ikonomov, O. C., Strakova, J., Dondapati, R., Mlak, K., Deeb, R., Silver, R., and Shisheva, A. (2004) A mammalian ortholog of *Saccharomyces cerevisiae* Vac14 that associates with and up-regulates PIKfyve phosphoinositide 5-kinase activity. *Mol. Cell. Biol.* **24,** 10437–10447
20. Zolov, S. N., Bridges, D., Zhang, Y., Lee, W. W., Riehle, E., Verma, R., Lenk, G. M., Converso-Baran, K., Weide, T., Albin, R. L., Saltiel, A. R., Meisler, M. H., Russell, M. W., and Weisman, L. S. (2012) *In vivo*, Pikfyve generates PI(3,5)P2, which serves as both a signaling lipid and the major precursor for PI5P. *Proc. Natl. Acad. Sci. U.S.A.* **109,** 17472–17477
21. Chow, C. Y., Zhang, Y., Dowling, J. J., Jin, N., Adamska, M., Shiga, K., Szigeti, K., Shy, M. E., Li, J., Zhang, X., Lupski, J. R., Weisman, L. S., and Meisler, M. H. (2007) Mutation of *FIG4* causes neurodegeneration in the pale tremor mouse and patients with CMT4J. *Nature* **448,** 68–72
22. Vaccari, I., Dina, G., Tronchère, H., Kaufman, E., Chicanne, G., Cerri, F., Wrabetz, L., Payrastre, B., Quattrini, A., Weisman, L. S., Meisler, M. H., and Bolino, A. (2011) Genetic interaction between MTMR2 and FIG4 phospholipid phosphatases involved in Charcot-Marie-Tooth neuropathies. *PLoS Genet.* **7,** e1002319
23. Engelender, S., Kaminsky, Z., Guo, X., Sharp, A. H., Amaravi, R. K., Kleiderlein, J. J., Margolis, R. L., Troncoso, J. C., Lanahan, A. A., Worley, P. F., Dawson, V. L., Dawson, T. M., and Ross, C. A. (1999) Synphilin-1 associates with α-synuclein and promotes the formation of cytosolic inclusions. *Nat. Genet.* **22,** 110–114
24. Szargel, R., Rott, R., and Engelender, S. (2008) Synphilin-1 isoforms in Parkinson's disease: regulation by phosphorylation and ubiquitylation. *Cell. Mol. Life Sci.* **65,** 80–88
25. Beyer, K., Domingo-Sàbat, M., and Ariza, A. (2009) Molecular pathology

of Lewy body diseases. *Int. J. Mol. Sci.* **10,** 724–745
26. Wakabayashi, K., Engelender, S., Yoshimoto, M., Tsuji, S., Ross, C. A., and Takahashi, H. (2000) Synphilin-1 is present in Lewy bodies in Parkinson's disease. *Ann. Neurol.* **47,** 521–523
27. Katsuse, O., Iseki, E., Marui, W., and Kosaka, K. (2003) Developmental stages of cortical Lewy bodies and their relation to axonal transport blockage in brains of patients with dementia with Lewy bodies. *J. Neurol. Sci.* **211,** 29–35
28. Sbrissa, D., Ikonomov, O. C., and Shisheva, A. (1999) PIKfyve, a mammalian ortholog of yeast Fab1p lipid kinase, synthesizes 5-phosphoinositides: effect of insulin. *J. Biol. Chem.* **274,** 21589–21597
29. Ikonomov, O. C., Sbrissa, D., Ijuin, T., Takenawa, T., and Shisheva, A. (2009) Sac3 is an insulin-regulated phosphatidylinositol 3,5-bisphosphate phosphatase: gain in insulin responsiveness through Sac3 down-regulation in adipocytes. *J. Biol. Chem.* **284,** 23961–23971
30. Shisheva, A., Doxsey, S. J., Buxton, J. M., and Czech, M. P. (1995) Pericentriolar targeting of GDP-dissociation inhibitor isoform 2. *Eur. J. Cell Biol.* **68,** 143–158
31. Ikonomov, O. C., Sbrissa, D., Dondapati, R., and Shisheva, A. (2007) ArPIKfyve-PIKfyve interaction and role in insulin-regulated GLUT4 translocation and glucose transport in 3T3-L1 adipocytes. *Exp. Cell Res.* **313,** 2404–2416
32. Sanderson, T. H., Raghunayakula, S., and Kumar, R. (2015) Neuronal hypoxia disrupts mitochondrial fusion. *Neuroscience* **301,** 71–78
33. Feng, H. Z., Chen, X., Hossain, M. M., and Jin, J. P. (2012) Toad heart utilizes exclusively slow skeletal muscle troponin T: an evolutionary adaptation with potential functional benefits. *J. Biol. Chem.* **287,** 29753–29764
34. Chen, X., Walker, A. K., Strahler, J. R., Simon, E. S., Tomanicek-Volk, S. L., Nelson, B. B., Hurley, M. C., Ernst, S. A., Williams, J. A., and Andrews, P. C. (2006) Organellar proteomics: analysis of pancreatic zymogen granule membranes. *Mol. Cell. Proteomics* **5,** 306–312
35. O'Farrell, C., Pickford, F., Vink, L., McGowan, E., and Cookson, M. R. (2002) Sequence conservation between mouse and human synphilin-1. *Neurosci. Lett.* **322,** 9–12
36. Nagano, Y., Yamashita, H., Takahashi, T., Kishida, S., Nakamura, T., Iseki, E., Hattori, N., Mizuno, Y., Kikuchi, A., and Matsumoto, M. (2003) Siah-1 facilitates ubiquitination and degradation of synphilin-1. *J. Biol. Chem.* **278,** 51504–51514
37. Bandopadhyay, R., Kingsbury, A. E., Muqit, M. M., Harvey, K., Reid, A. R., Kilford, L., Engelender, S., Schlossmacher, M. G., Wood, N. W., Latchman, D. S., Harvey, R. J., and Lees, A. J. (2005) Synphilin-1 and Parkin show overlapping expression patterns in human brain and form aggresomes in response to proteasomal inhibition. *Neurobiol. Dis.* **20,** 401–411
38. O'Farrell, C., Murphy, D. D., Petrucelli, L., Singleton, A. B., Hussey, J., Farrer, M., Hardy, J., Dickson, D. W., and Cookson, M. R. (2001) Transfected synphilin-1 forms cytoplasmic inclusions in HEK293 cells. *Brain Res. Mol. Brain Res.* **97,** 94–102
39. Zaarur, N., Meriin, A. B., Gabai, V. L., and Sherman, M. Y. (2008) Triggering aggresome formation: dissecting aggresome-targeting and aggregation signals in synphilin 1. *J. Biol. Chem.* **283,** 27575–27584
40. Ferguson, C. J., Lenk, G. M., and Meisler, M. H. (2009) Defective autophagy in neurons and astrocytes from mice deficient in PI(3,5)P2. *Hum. Mol. Genet.* **18,** 4868–4878
41. Eyal, A., and Engelender, S. (2006) Synphilin isoforms and the search for a cellular model of Lewy body formation in Parkinson's disease. *Cell Cycle* **5,** 2082–2086
42. Wong, E., Bejarano, E., Rakshit, M., Lee, K., Hanson, H. H., Zaarur, N., Phillips, G. R., Sherman, M. Y., and Cuervo, A. M. (2012) Molecular determinants of selective clearance of protein inclusions by autophagy. *Nat. Commun.* **3,** 1240
43. Hsiao, V. C., Tian, R., Long, H., Der Perng, M., Brenner, M., Quinlan, R. A., and Goldman, J. E. (2005) Alexander-disease mutation of GFAP causes filament disorganization and decreased solubility of GFAP. *J. Cell Sci.* **118,** 2057–2065
44. Quinlan, R. A., Brenner, M., Goldman, J. E., and Messing, A. (2007) GFAP and its role in Alexander disease. *Exp. Cell Res.* **313,** 2077–2087
45. Lee, G., Junn, E., Tanaka, M., Kim, Y. M., and Mouradian, M. M. (2002) Synphilin-1 degradation by the ubiquitin-proteasome pathway and effects on cell survival. *J. Neurochem.* **83,** 346–352
46. Tanji, K., Tanaka, T., Mori, F., Kito, K., Takahashi, H., Wakabayashi, K., and Kamitani, T. (2006) NUB1 suppresses the formation of Lewy body-like inclusions by proteasomal degradation of synphilin-1. *Am. J. Pathol.* **169,** 553–565
47. Klionsky, D. J., and Ohsumi, Y. (1999) Vacuolar import of proteins and organelles from the cytoplasm. *Annu. Rev. Cell Dev. Biol.* **15,** 1–32
48. Ikonomov, O. C., Sbrissa, D., Venkatareddy, M., Tisdale, E., Garg, P., and Shisheva, A. (2015) Class III PI 3-kinase is the main source of PtdIns3P substrate and membrane recruitment signal for PIKfyve constitutive function in podocyte endomembrane homeostasis. *Biochim. Biophys. Acta* **1853,** 1240–1250
49. Kon, T., Mori, F., Tanji, K., Miki, Y., Toyoshima, Y., Yoshida, M., Sasaki, H., Kakita, A., Takahashi, H., and Wakabayashi, K. (2014) ALS-associated protein FIG4 is localized in Pick and Lewy bodies, and also neuronal nuclear inclusions, in polyglutamine and intranuclear inclusion body diseases. *Neuropathology* **34,** 19–26
50. Wakabayashi, K., Tanji, K., Odagiri, S., Miki, Y., Mori, F., and Takahashi, H. (2013) The Lewy body in Parkinson's disease and related neurodegenerative disorders. *Mol. Neurobiol.* **47,** 495–508
51. Kalia, L. V., Kalia, S. K., McLean, P. J., Lozano, A. M., and Lang, A. E. (2013) α-Synuclein oligomers and clinical implications for Parkinson disease. *Ann. Neurol.* **73,** 155–169
52. Sharma, S., Moon, C. S., Khogali, A., Haidous, A., Chabenne, A., Ojo, C., Jelebinkov, M., Kurdi, Y., and Ebadi, M. (2013) Biomarkers in Parkinson's disease (recent update). *Neurochem. Int.* **63,** 201–229
53. Xu, W., Tan, L., and Yu, J. T. (2015) The link between the *SNCA* gene and parkinsonism. *Neurobiol. Aging* **36,** 1505–1518
54. Smith, W. W., Margolis, R. L., Li, X., Troncoso, J. C., Lee, M. K., Dawson, V. L., Dawson, T. M., Iwatsubo, T., and Ross, C. A. (2005) α-Synuclein phosphorylation enhances eosinophilic cytoplasmic inclusion formation in SH-SY5Y cells. *J. Neurosci.* **25,** 5544–5552
55. Drouet, V., and Lesage, S. (2014) Synaptojanin 1 mutation in Parkinson's disease brings further insight into the neuropathological mechanisms. *BioMed Res. Int.* **2014,** 289728
56. Bonifati, V. (2012) Autosomal recessive parkinsonism. *Parkinsonism Relat. Disord.* **18,** Suppl. 1, S4–S6
57. Zhang, Y., Granholm, A. C., Huh, K., Shan, L., Diaz-Ruiz, O., Malik, N., Olson, L., Hoffer, B. J., Lupica, C. R., Hoffman, A. F., and Bäckman, C. M. (2012) PTEN deletion enhances survival, neurite outgrowth, and function of dopamine neuron grafts to MitoPark mice. *Brain* **135,** 2736–2749
58. Ikonomov, O. C., Filios, C., Sbrissa, D., Chen, X., and Shisheva, A. (2013) The PIKfyve-ArPIKfyve-Sac3 triad in human breast cancer: functional link between elevated Sac3 phosphatase and enhanced proliferation of triple negative cell lines. *Biochem. Biophys. Res. Commun.* **440,** 342–347
59. Farrer, M., Kachergus, J., Forno, L., Lincoln, S., Wang, D. S., Hulihan, M., Maraganore, D., Gwinn-Hardy, K., Wszolek, Z., Dickson, D., and Langston, J. W. (2004) Comparison of kindreds with parkinsonism and α-synuclein genomic multiplications. *Ann. Neurol.* **55,** 174–179
60. Kara, E., Kiely, A. P., Proukakis, C., Giffin, N., Love, S., Hehir, J., Rantell, K., Pandraud, A., Hernandez, D. G., Nacheva, E., Pittman, A. M., Nalls, M. A., Singleton, A. B., Revesz, T., Bhatia, K. P., Quinn, N., Hardy, J., Holton, J. L., and Houlden, H. (2014) A 6.4 Mb duplication of the α-synuclein locus causing frontotemporal dementia and Parkinsonism: phenotype-genotype correlations. *JAMA Neurol.* **71,** 1162–1171
61. Muenter, M. D., Forno, L. S., Hornykiewicz, O., Kish, S. J., Maraganore, D. M., Caselli, R. J., Okazaki, H., Howard, F. M., Jr., Snow, B. J., and Calne, D. B. (1998) Hereditary form of parkinsonism-dementia. *Ann. Neurol.* **43,** 768–781
62. Gwinn, K., Devine, M. J., Jin, L. W., Johnson, J., Bird, T., Muenter, M., Waters, C., Adler, C. H., Caselli, R., Houlden, H., Lopez, G., Singleton, A., Hardy, J., and Singleton, A. (2011) Clinical features, with video documentation, of the original familial Lewy body parkinsonism caused by α-synuclein triplication (Iowa kindred). *Mov. Disord.* **26,** 2134–2136
63. Houlden, H., and Singleton, A. B. (2012) The genetics and neuropathology of Parkinson's disease. *Acta Neuropathol.* **124,** 325–338

64. Swinnen, E., , S., Outeiro, T. F., Galas, M. C., Madeo, F., Winderickx, J., and Franssens, V. (2011) Aggresome formation and segregation of inclusions influence toxicity of α-synuclein and synphilin-1 in yeast. *Biochem. Soc. Trans.* **39,** 1476–1481
65. Volpicelli-Daley, L. A., Gamble, K. L., Schultheiss, C. E., Riddle, D. M., West, A. B., and Lee, V. M. (2014) Formation of α-synuclein Lewy neurite-like aggregates in axons impedes the transport of distinct endosomes. *Mol. Biol. Cell* **25,** 4010–4023
66. Volpicelli-Daley, L. A., Luk, K. C., Patel, T. P., Tanik, S. A., Riddle, D. M., Stieber, A., Meaney, D. F., Trojanowski, J. Q., and Lee, V. M. (2011) Exogenous α-synuclein fibrils induce Lewy body pathology leading to synaptic dysfunction and neuron death. *Neuron* **72,** 57–71
67. Jin, H. G., Yamashita, H., Nakamura, T., Fukuba, H., Takahashi, T., Hiji, M., Kohriyama, T., and Matsumoto, M. (2008) Synphilin-1 transgenic mice exhibit mild motor impairments. *Neurosci. Lett.* **445,** 12–17
68. Krenz, A., Falkenburger, B. H., Gerhardt, E., Drinkut, A., and Schulz, J. B. (2009) Aggregate formation and toxicity by wild-type and R621C synphilin-1 in the nigrostriatal system of mice using adenoviral vectors. *J. Neurochem.* **108,** 139–146
69. Nuber, S., Franck, T., Wolburg, H., Schumann, U., Casadei, N., Fischer, K., Calaminus, C., Pichler, B. J., Chanarat, S., Teismann, P., Schulz, J. B., Luft, A. R., Tomiuk, J., Wilbertz, J., Bornemann, A., Krüger, R., and Riess, O. (2010) Transgenic overexpression of the α-synuclein interacting protein synphilin-1 leads to behavioral and neuropathological alterations in mice. *Neurogenetics* **11,** 107–120
70. Opazo, F., Krenz, A., Heermann, S., Schulz, J. B., and Falkenburger, B. H. (2008) Accumulation and clearance of α-synuclein aggregates demonstrated by time-lapse imaging. *J. Neurochem.* **106,** 529–540